

Beam Test Results for the sPHENIX Electromagnetic and Hadronic Calorimeter Prototypes.

Abstract

The electromagnetic calorimeter and hadronic calorimeter design for the proposed sPHENIX detector at the Relativistic Heavy Ion Collider (RHIC) were tested at the Fermilab Test Beam Facility as part of experiment T-1044 in the spring of 2016. The sPHENIX experiment is designed to measure jets in heavy ion collisions to probe the properties of the Quark-Gluon Plasma (QGP). To achieve the goals of the proposed physics program, an energy resolution of $15\%/\sqrt{E}$ and $100\%/\sqrt{E}$ are required for the electromagnetic and hadronic calorimeters, respectively. The test beam results of a prototype of the scintillating fibers embedded in tungsten design of the EMCal and the alternating layers of tilted steel plate and scintillator plates design of the HCal demonstrate that the proposed sPHENIX calorimeter system is within the sPHENIX specifications. The results are also shown to be consistent with GEANT4 simulations.

Keywords: RHIC, sPHENIX, Electromagnetic Calorimetry, Hadronic Calorimetry, SpaCal, SiPM, Prototypes

1. Introduction

sPHENIX is a proposed general purpose detector at the Relativistic Heavy Ion Collider (RHIC), which collides gold ions at $\sqrt{s_{NN}} = 200$ GeV to create the hot dense matter known as the Quark Gluon Plasma (QGP) [1, 2, 3, 4]. sPHENIX is especially designed to measure the collimated spray of particles known as jets resulting from hard scatterings that occur early in the collision process to probe the properties of the QGP. To reconstruct the jets and study their constituents, sPHENIX comprises calorimeters and tracking system which have full 2π acceptance in azimuth and a pseudorapidity coverage of $|\eta| < 1$. This article discusses the prototype of one sector of the sPHENIX calorimeters that was built and tested in preparation of the full construction.

The sPHENIX calorimeter system comprises an electromagnetic calorimeter and an inner hadronic calorimeter, which sit inside a solenoid magnet, in addition to the outer hadronic calorimeter located outside of the magnet. The electromagnetic calorimeter is important for identifying photons and electrons. Photons can be used to tag the energy of opposing jets in the QGP and electrons are important for Υ suppression and heavy flavor jet measurements. The hadronic calorimeters are necessary for capturing the hadronic component of the jets. To accurately measure the energy resolution of the sPHENIX calorimeter system, a prototype was built and tested using the Test Beam Facility at Fermilab.

2. Prototype Electromagnetic Calorimeter

The electromagnetic calorimeter (EMCal) is designed based on both mechanical constraints and physics requirements. The principle mechanical constraint for the EMCal is that it must be compact—it must fit inside the BaBar magnet with enough space remaining for a tracking system. One major physics requirement is that it needs to have a large solid angle and be projective in two dimensions to enable accurate jet measurements. The second major physics requirement is for the EMCal resolution and segmentation to be compatible. This means that the cluster reconstruction should not be limited by the underlying heavy ion event background. For example, if a cluster from a 5 GeV electron (e.g. from a Υ decay) is measured, the typical cluster size is about 340 MeV. The EMCal resolution should therefore be $\leq 15\%/\sqrt{E}$.

The basic EMCal tower design is scintillating fibers embedded in the absorber material, which is a matrix of tungsten powder infused with epoxy (W/SciFi). This design was first tested by the UCLA group [5, 6] and is similar to the SPACAL design used in a number of experiments [7, 8, 9, 10, 11]. The SPACAL blocks are two tower blocks tapered in one-dimension (1D projective).

The scintillating fibers have a diameter of 0.47 mm and are held in position by a set of metal meshes with a nominal center to center spacing of 1.0 mm. The fiber assembly is encapsulated in absorber material, which is compacted by either by vibration to achieve a density of $\approx 10 \text{ g/cm}^3$. At that density the sampling fraction is expected to be 2.3% and the radiation length $X_0 \approx 7 \text{ mm}$. The blocks are made projective in one dimension by tilting the meshes progressively to bring the fibers closer together at the front of each block and create a taper. The back of the block has a height

Parameter	Units	Value
Inner radius (envelope)	mm	900
Outer radius (envelope)	mm	1161
Length (envelope)	mm	$2 \times 1495 = 2990$
tower length (absorber)	mm	144
Number of towers in azimuth ($\Delta\phi$)		256
Number of towers in pseudorapidity ($\Delta\eta$)		$2 \times 48 = 96$
Number of electronic channels (towers)		$256 \times 96 = 24576$
Number of SiPMs per tower		4
Number of towers per module		$2 \times 8 = 16$
Number of modules per sector		24
Number of towers per sector		384
Number of sectors		$2 \times 32 = 64$
Sector weight (estimated)	kg	326
Total weight (estimated)	kg	20890
Average sampling fraction		2.3%

Table 1: Key parameters of the EMCal

of 2.39 cm, the front has a height of 2.07 cm, and the total length of the blocks is 13.9 cm.

The EMCal described here consists of 32 such blocks for a total of 64 towers. Each tower is equipped with a lightguide on the front face and read out by four silicon photomultipliers (SiPMs) passively summed into a single preamp/electronics channel.

When fully constructed, the EMCal will consist of 64 sectors (32 azimuthal \times 2 longitudinal) supported by the inner hadronic calorimeter. Each sector will subtend 11.2° in ϕ and cover 1.1 units in η . Table 1 gives the key parameters for the EMCal.

2.1. EMCal Module Production

The EMCal W/SciFi block construction is similar to the construction of the two-tower blocks tapered in one dimension (1D projective) SPACAL blocks developed at UCLA. The basic materials, as discussed above, are described in detail in Table 2. The scintillating fibers are placed inside of the brass mesh screens, positioning the fibers. The screens are then separated and placed into a mold and are tilted to form the taper in one direction, as shown in Figure 1a. Tungsten powder is poured uniformly into the mold, which is vibrated at the same time to insure uniformity.

70 Epoxy is then poured into the W/SciFi matrix and light vacuum is applied
until the epoxy is seen in the three ports at the bottom of the mold; see
Figure 1b. After 24 hours, the W/SciFi block is released from the mold,
and then machined using a technique developed at UIUC which first cuts
the blocks with carbide tips, and then a diamond tip. This allows for the
ends of the blocks to be cut without damaging the fibers; see Figure 1c.
75 The final W/SciFi 1×2 1D projective block is shown in Figure 1d.

Material	Property	Value
Tungsten powder	THP Technon 100 mesh	
	Particle size	$\leq 100 \mu\text{m}$
	bulk density (solid)	$\geq 18.50 \text{ g/cm}^3$
	tap density (powder)	$\geq 11.25 \text{ g/cm}^3$
	purity	≥ 99.9 percent W
Scintillating fiber	impurities (≤ 0.1 percent)	Fe, Ni, O2 , Co, Cr, Cu, Mo
	Kuraray SCSF78 (blue)	
	fiber diameter	0.47 mm
	cladding	single
	core material	polystyrene
	cladding material	polymethylmethacrylate
	emission peak	450 nm
	decay time	2.8 ns
	attenuation length	$\geq 4.0 \text{ m}$
Epoxy	Epo-Tek 301	
	pot life	1-2 hours
	index of refraction	1.519 at 589 nm
	spectral transmission	$\geq 99 \%$ at 382-980 nm

Table 2: EMCal module component materials

2.2. Light Collection

The starting design for the EMCal light guide is the design developed
by Oleg Tsai for the UCLA SPACAL prototypes. This is a machined
acrylic trapezoidal shape that fully covers one tower of the W/SciFi block
80 ($26.4 \times 23.6 \text{ mm}^2$) and transitions over a 25.4 mm height to an area large
enough ($14 \times 14 \text{ mm}^2$) to accommodate a 2×2 array of SiPMs, see Fig-
ure 2.

The optical transmission of a sample UCLA light guide and a one inch
cube of the same material are presented in Figure 3a. The transmission



(a)

Scintillating fibers held by metal meshes



(b)

Tungsten powder and epoxy added



carbide tip

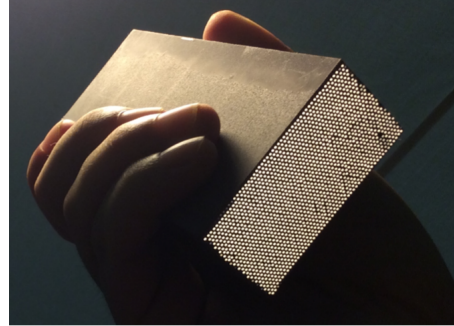


diamond tip



(c)

Finished modules are diamond cut



(d)

Final EMCal block

Figure 1: EMCal module production. a) The scintillating fibers are placed in an aluminum mold with a 3D printed bottom, held by metal meshes to keep the fibers in place. b) After Tungsten powder is added, epoxy is poured uniformly over the mold where it dries for 24 hours. c) The modules are machined with carbide and diamond tips. d) The final module. e) The stack of completed modules along with the light guides in the second row. f) The first assembly of the module including light guides and SiPMs.

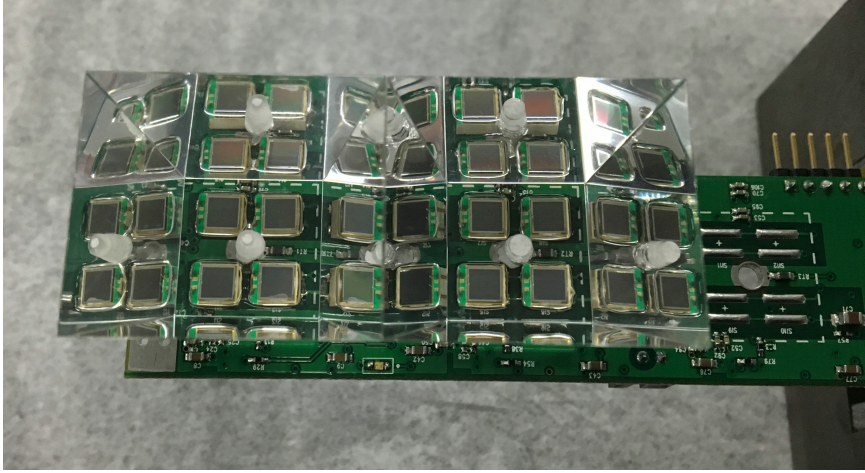


Figure 2: SPACAL acrylic light guides and SiPM array.

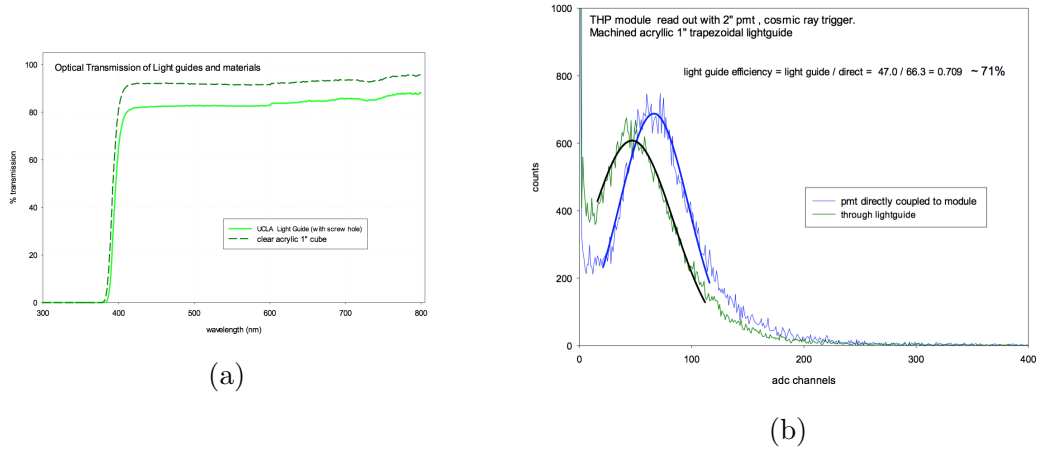


Figure 3: (a) Optimal transmission of light guides, and (b) Light guide efficiency.

85 measurement is sensitive to the tapped hole for the SiPM mounting, since
the spectrometer beam passes through the face. The SiPMs are mounted
around the hole, and are therefore less affected. The acrylic transmits 92%
of the light with an emission peak of 450 nm.

The light guides are epoxied to the thin end of the 1×2 tower block.
90 Four SiPMs, mounted on an EMCal 1×8 board are used to read out
the block. The SiPMs are coupled to the light guide using optical grease.
Trigger counters are positioned above and below the block. The summed
signals from the four SiPMs are integrated in an ADC and the light output
peak is measured.

95 To measure the overall efficiency of the light guide, one tower of a
W/SciFi block is optically coupled to a 2 inch window photomultiplier tube
(PMT). The PMT window fully covers the readout surface of the block,
and the readout end of the tower is masked. The cosmic peak position is
measured in an ADC, with cosmic trigger counters above and below the
100 block. An acrylic light guide is optically coupled between the block and the
PMT, and the measurement is repeated. Relative to the directly coupled
measurement, the light guide measurement yields 71 % of the light, which
represents the total efficiency of the light guide. This efficiency is insensitive
to any non-uniformities in the distribution of light from the block and also
105 the collection or transmission of light to the PMT. The measured relative
collective efficiency is shown in Figure 4.

An upper limit on the Cherenkov background in the light guides is es-
timated from the test beam data. With the EMCal rotated 90 degrees
downward from its nominal position and the beam centered horizontally on
110 a column, data was collected with the beam centered at various vertical
positions. Events are selected by requiring a minimum energy on an indi-
vidual vertical hodoscope finger and no energy above the pedestal for all
towers, except for towers centered on the beam. The Cherenkov background
is observed in the energy distribution when the beam is at vertical positions
115 associated with the light guides, whereas, energy distributions similar to
the above MIP calibration are observed at vertical positions associated with
the modules. The mean energy from the Cherenkov background, $\langle E \rangle$, plus
 $1.281 \cdot \text{RMS}/\sqrt{\text{events}}$ is divided by the mean energy from the module
distributions to estimate the upper limit of the Cherenkov background con-
120 tribution to be $< 11\%$. Since the beam hits the light guides perpendicular
to their nominal position, the Cherenkov background will be significantly
smaller during physics data acquisition than this estimated upper limit.

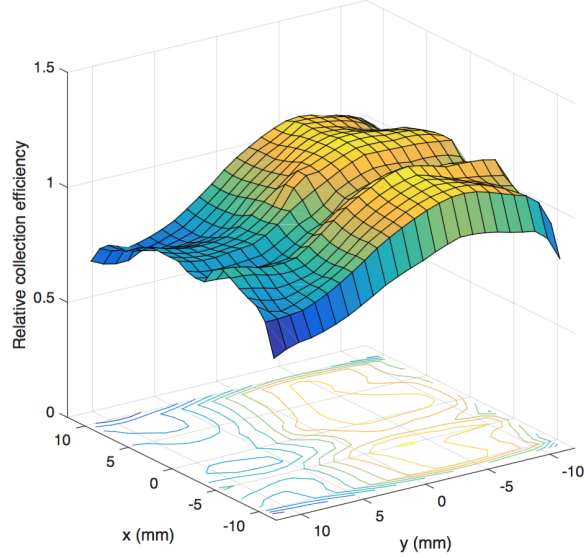


Figure 4: Measured Collective Light Guide Efficiency

2.3. Assembly and Support

The assembly of the modules from both THP and UIUC was completed at BNL before finally being shipped at Fermilab for the test beam. The blocks were first epoxied together into rows of 8 towers in a gluing fixture, which aligned the front readout surface of the blocks in a single plane. Two layers of Vikuiti ESR reflective film were then epoxied to the back surface of each of the rows. Once cured, light guides were epoxied to the front surface of the row. The preamp PCB was used to align the light guides on the towers. The SiPMs were sorted into groups of four, to minimize the spread in the gains of the devices on any tower. They were then soldered onto the preamp pcb in groups of four. The SiPMs were optically coupled to the light guides using GE Silicones RTV615 silicone, with the PCB mechanically secured through a screw to the center of each tower light guide, see Figure 6.

3. Prototype Hadronic Calorimeter

The hadronic calorimeter (HCal) is a sampling calorimeter with two radial segments: one inside the magnet and another outside the magnet.

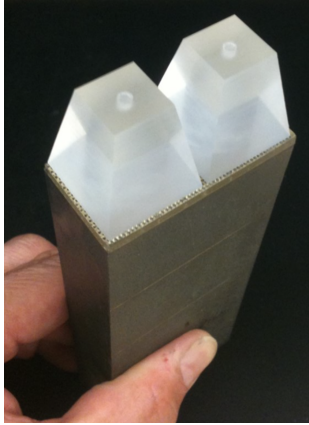


Figure 5: EMCal 2 tower block with light guides

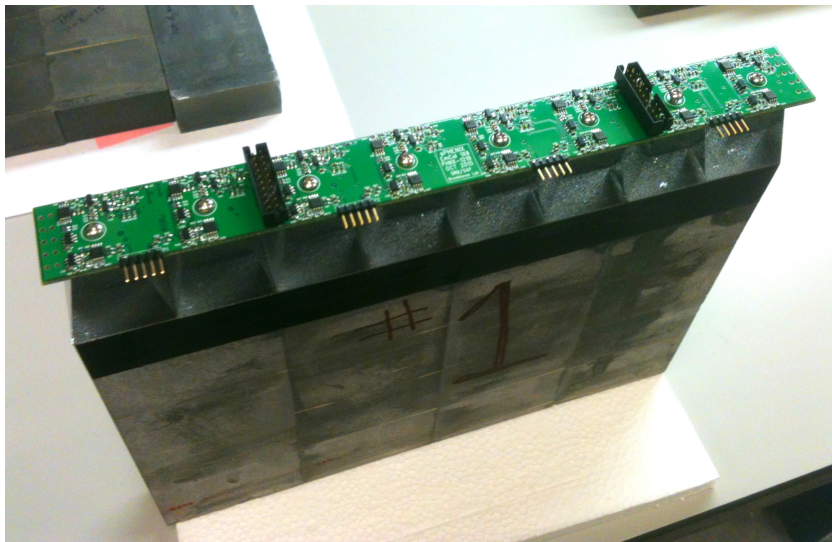


Figure 6: EMCal row of blocks with light guides and preamp board

140 The outer hadronic calorimeter additionally serves as the flux return of the magnet. The performance requirement of the sPHENIX HCal is driven by the physics requirements related to measuring jets in relativistic heavy ion collisions. At the jet energies of interest for the sPHENIX physics program, the energy resolution is dominated by the underlying event, not the energy
 145 resolution of the HCal, therefore the required energy resolution is a relatively modest $\sigma/E < 100\%/\sqrt{E}$.

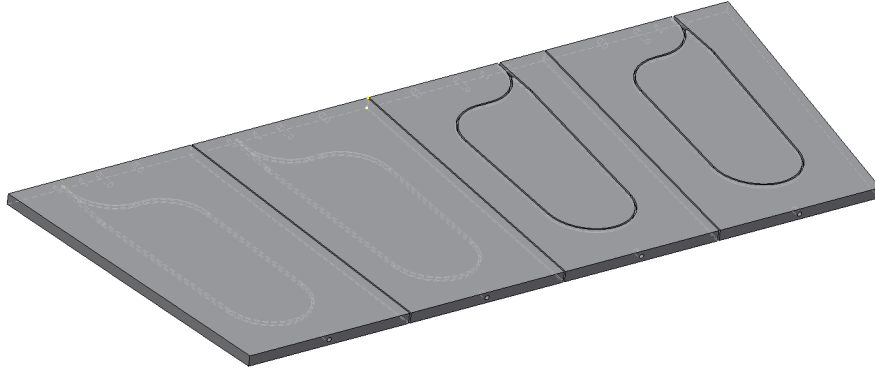
The inner and outer HCal prototypes are constructed as a small azimuthal segment of the full scale sPHENIX design, with alternating layers of scintillator tiles and steel absorber plates. The absorber plates are tapered and tilted from the radial direction to provide more uniform sampling
 150 in azimuth. Extruded tiles of plastic scintillator with an embedded wavelength shifting fiber are interspersed between the absorber plates. The tilt angle is chosen so that a radial track from the center of the interaction region traverses at least four scintillator tiles. Each tile is read out at the
 155 outer radius with SiPMs. The analog signals from five tiles are ganged to a single preamplifier channel to form a single calorimeter tower. A block of three aluminum plates is inserted between the inner and outer prototypes to represent the magnet.

The properties of the HCal scintillating tiles are listed in Table 3. These
 160 tiles are similar to the design of scintillators for the T2K experiment by the INR group (Troitsk, Russia) and the MINOS experiment [12]. Figure 7(a) shows the steps of tile production. First the plastic scintillator tiles are machined, coated, and then a groove is cut into the tiles such that the wavelength shifting fiber can be embedded. The fiber routing is designed so
 165 that any energy deposited in the scintillator is within 2.5 cm of a WLS fiber, and the bend radius of any turn in the fiber has been limited to 35 mm to prevent excess mechanical stress and light loss based on T2K and our own empirical experience with test tiles. Figure 7(a,b) and Figure 8 shows the inner and outer HCal fiber routing patterns. The Kuraray single clad fiber
 170 is chosen due to its flexibility and longevity, both of which are critical in the geometry with multiple fiber bends. The properties of the HCal wavelength shifting fibers are listed in Table 4.

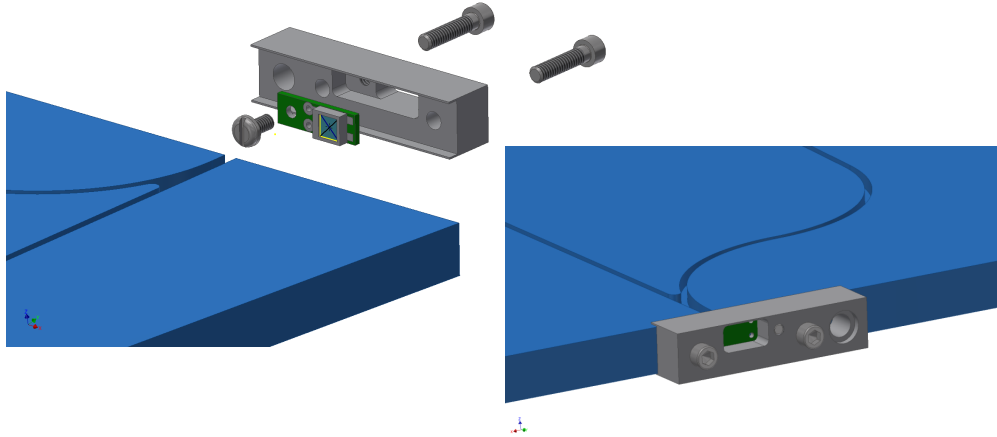
The scintillating light produced in the tiles by ionization from charged particles is kept inside the tile and reflected diffusely by a reflective coating
 175 and reflective tile wrapping. The light is absorbed by the fiber embedded in the scintillator. As shown in Figure 7(c), the two ends of the fiber are brought to the outer radius of the tile where a small plastic mount supports



(a) Scintillator tile production for inner HCal



(b) Inner HCal tile design patterns



(c) Plastic coupler to attach the SiPM at the fiber exit

Figure 7: HCal tile production. (a) Scintillator tiles are machined, coated and embedded with WLS fibers. (b) 4 scintillating tiles arranged in η direction between steel absorber plates. (c) SiPM installation at the fiber exit using a plastic coupler.

Property	
Plastic	Extruded polystyrene
Scintillation dopant	1.5% of PTP and 0.01% POPOP
Reflective coating	Proprietary coating by surface exposure to aromatic solvents
Reflective layer thickness	50 μm
Wrapping	0.1 mm Al foil followed by one layer of 30 μm cling-wrap and a 100 μm layer of black TED-LAR
Attenuation length in lateral (with respect to extrusion) direction	≈ 30 mm
Wavelength shifting fiber	Single clad Kuraray Y11
Fiber size	1 mm round
Fiber core attenuation length	> 2 m
Optical cement	Epotek 3015

Table 3: Properties of HCal scintillating tiles.

a $3 \times 3 \text{ mm}^2$ SiPM at the fiber exit. The fiber exit is orthogonal to the tile edge and glued at a depth in the tile that allows for installation of the SiPM centered around the fiber exits. An effort has been made to chose the gap between the fiber exits and the face of the SiPM to maximize the light spread over the SiPM surface to reduce the probability of optical saturation resulting from two or more photons impinging on the same pixel. The gap of 0.75 mm is chosen based on the requirements that no more than 5% variation in the SiPM response when fibers and SiPM are misaligned for 0.2 mm and no more than 20% loss of the light outside of SiPM sensitive area. We estimate that the expected 80% of the light is indeed collected from the fiber.

3.1. Tile construction

Scintillating tiles for the calorimeter are manufactured by the UNIPLAST Company in Vladimir, Russia. The dry mix of polystyrene granules, PTP, and POPOP is melted and extruded by an industrial extrusion machine which produces a continuous band of hot scintillating plastic 25 cm wide.

Property	
Fiber diameter	1.0 mm
Formulation	200, K-27, S-Type
Cladding	single
Cladding thickness	2 percent of d (0.02 mm)
Numerical Aperture (NA)	0.55
Emission angle	33.7 deg
Trapping Efficiency	3.1 percent
Core material	polystyrene (PS)
Core density	1.05 g/cc
Core refractive index	1.59
Cladding material	Polymethylmethacrylate (PMMA)
Cladding density	1.19 g/cc
Cladding refractive index	1.49
Color	green
Emission peak	476 nm
Absorption Peak	430 nm
Attenuation length	> 3.5 m
Minimum bending radius	100 mm

Table 4: Properties of Kuraray Y-11 (200) wavelength shifting fibers.

195 The scintillator is then cut into 2 m long pieces which are inspected for
 defects and miscolorations and, if this low level control is passed, mechan-
 ically machined into the tiles according to the drawings. The tiles are the
 placed in a bath of a mix of aromatic solvents resulting in the development of
 a white diffuse reflective coating over the whole tile surface with an average
 200 thickness of 0.05 mm. This process removes microscopic non-uniformities
 normally present on the surface of extruded plastic thus decreasing aging
 and improving tile ability to withstand pressure without crazing. It also en-
 hances the efficiency of light collection in tiles with embedded WLS fibers.
 Coated tiles are grooved, then WSF are embedded and glued using optical
 205 epoxy (EPOTEC-301) with special care given to fiber positioning at the
 exit from the tile. The fibers are cut at the tile edge and polished by hand.

3.2. Tile testing

To determine the light response across the tiles, various studies have
 been performed. One such study, both long term and ongoing, has been
 210 conducted at the University of Colorado at Boulder (CU Boulder). In that

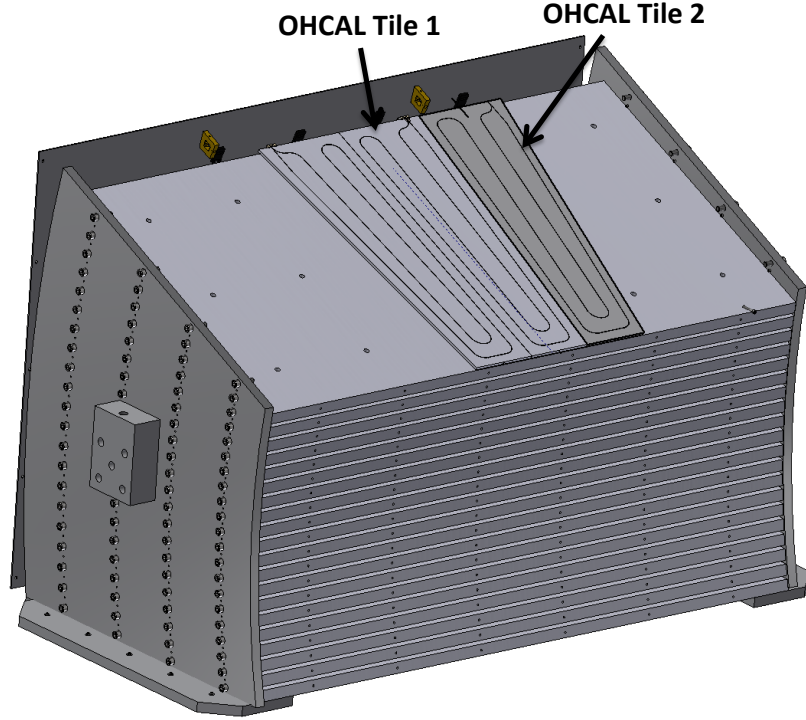


Figure 8: Outer HCal tile designs and assembly

experimental setup, an LED with a collimator is attached to a container on a two-dimensional rail system with very accurate stepper motors for each. This allows an automated analysis with very high positional precision. The LED scans of the outer HCal tiles consist of 174 points in the long direction (X) and 54 points in the short direction (Y) for a total of 9,396 points. The scan positions are 5 mm apart in each direction. Although much finer position resolution is possible, the spot size of the collimated LED light is of order 5 mm such that finer position resolution would not provide any additional information. The principle disadvantage of an LED scan is that light is inserted into the tile directly rather than being induced by ionizing radiation.

During the test beam running, a “Tile Mapper” was constructed and placed on the motion table in area MT6.2C of the experiment hall. This enabled a detailed study of the light response as a function of position. The scan consisted of 20 total positions, 10 positions focused on the inner part

of the tile and 10 focused on the outer part of the tile. A few of the outer scan positions fall near the edge and are excluded from the analysis.

Figure 9 shows the scan positions (represented as black circles) overlaid on an LED scan of a different tile performed at CU Boulder. The relative positional accuracy of the points is 2-3 mm. The numbers show the ratio of the average ADC value of the 16 GeV pion data to the average ADC value of the LED scan for that point. The normalization is arbitrarily chosen so that the numerical values are near unity.

It can be seen that most of the points from the 16 GeV pion data agree with the LED data very well. The points very close to the SiPM, which can be seen as the red region in the upper left, show a downward trend, suggesting that the intense bright spot in the LED data is not seen to be as intense in the 16 GeV pion data. Additionally, the lower set of the 5 inner points are systematically a little lower than the LED data, and they appear to be right on top of the fiber. This is most likely due to the fact that, in the LED scan, some of the light from the LED is captured directly by the fiber, so that there's a modest enhancement directly over the fiber that is naturally not present in the 16 GeV pion data. Both sets of 5 inner points, however, show decreasing trend as the points get close to the SiPM.

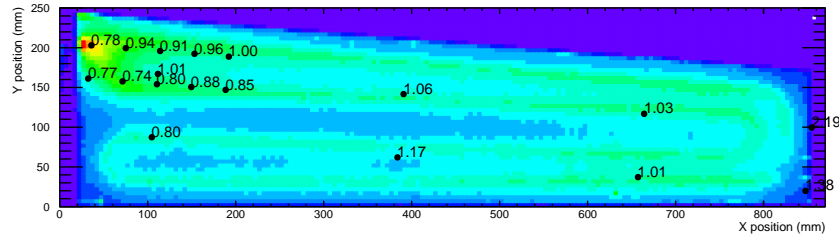


Figure 9: LED tile response with tile mapper scan data overlaid.

Figure 10 shows the average ADC value for each scan position as a function of the distance from the SiPM. As discussed above, the 16 GeV pion data do not show as much of an enhancement near the SiPM as the LED scan. However, it can be very clearly seen that for points less than 150 mm away from the SiPM that there is a very strong rise in the average ADC as the distance to the SiPM decreases. This is most likely due to the fact that some of the light in the fiber is carried in the cladding, which has a very short attenuation length, and is therefore lost for most positions in the tile. This is consistent with many studies, including those conducted at CU

255 Boulder as well as Abilene Christian University, that have demonstrated that a significant amount of the light (up to 50%) is carried in the cladding of the fiber.

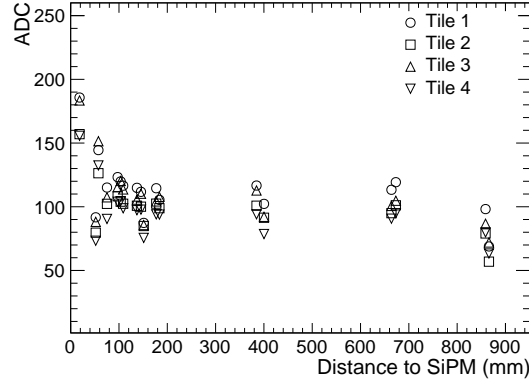


Figure 10: Average ADC value in the tile as a function of distance from the SiPM.

3.3. Geometry

A schematic diagram of the full test beam setup including the EMCal and HCal prototypes is shown in Figure 11. The inner HCal occupies a radial envelope bounded by 50 mm clearance inside the solenoid cryostat and the outer radius of the electromagnetic calorimeter. Table 5 shows the basic mechanical parameters of the inner HCal prototype. The major components are 20 stainless steel absorber plates and 80 scintillating tiles which are read out with SiPMs along the inner radius of the detector. The SiPMs from five tiles are connected to a preamplifier. This resulted in total of 16 towers, 4 in ϕ and 4 in η , equipped with SiPM sensors, preamplifiers, and cables carrying the differential output of the preamplifiers to the digitizer system. Figure 12(a) shows the fully assembled inner HCal. 16 preamplifier boards corresponding to the 16 towers are clearly visible. In order to make the whole system light tight the front and back sides were covered with black cardboard during the entire data taking period.

For operational simplicity, we supply the same bias voltage to all 5 SiPMs in a given tower. For this reason, the SiPMs must be gain matched. The SiPMs are sorted and grouped to towers according to the manufacturer's measurements. The SiPM sensors, preamplifiers, and cables are arranged on

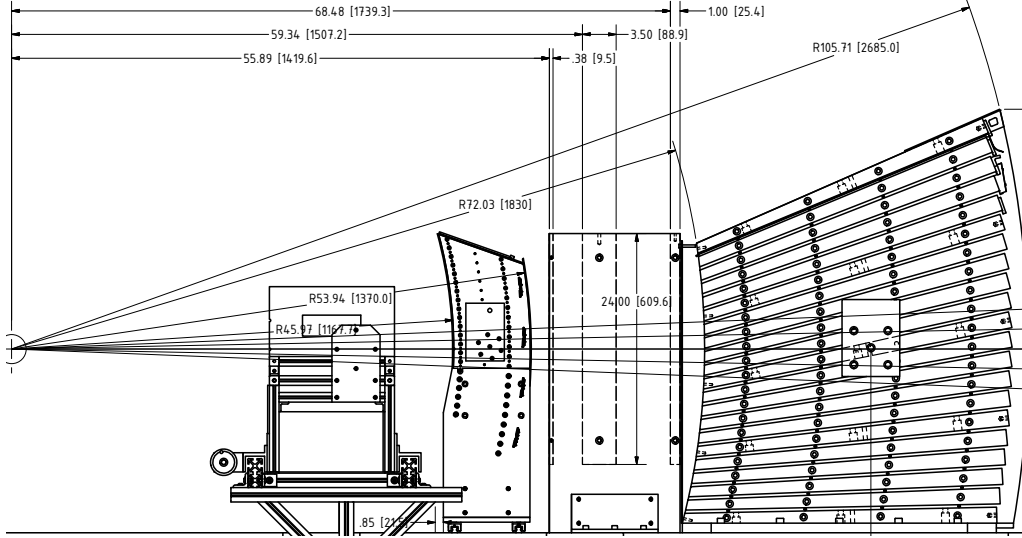


Figure 11: Schematic diagram of the testbeam setup. From left to right, it includes the EMCAL, inner HCal, cryostat, and outer HCal prototypes.

the inner circumference of the inner HCal. The interface board mounted on the side of the modules monitor the local temperatures and leakage currents, distribute the necessary voltages, and provide bias corrections for changes in temperature and leakage current.

280 Figure 12(b) shows the fully assembled outer HCal. The design of the outer HCal is similar to the inner HCal and the prototype is likewise comprised of 16 towers. However, since the absorber occupies considerably more radial space, in order to have a minimum thickness of $5.5\lambda_I$ a smaller tilt angle is needed to preserve the 4 crossing geometry. Table 6 summarizes
 285 the major design parameters of the outer HCal. The outer HCal SiPM sensors and electronics are to be arranged on the outer circumference of the detector.

3.4. Calibration

HCal calibration is performed using cosmic MIP events. A set of cosmic
 290 MIP events were recorded prior to the test beam data taking in order to calibrate the detector. The cosmic MIP events were triggered with scintillator paddles positioned at the top and bottom of the HCal (in the ϕ

Parameter	Units	Value
Inner radius (envelope)	mm	1157
Outer radius (envelope)	mm	1370
Length (envelope)	mm	??
Material	310 Stainless Steel	
Number of towers in azimuth ($\Delta\phi$)		4
Number of tiles per tower		5
Number of towers in pseudorapidity ($\Delta\eta$)		4
Number of electronic channels (towers)		$4 \times 4 = 16$
Module weight (estimated)	kg	900
Absorber plate thickness at inner radius	mm	10.2
Absorber plate thickness at outer radius	mm	14.7
Total number of absorber plates		21
Tilt angle (relative to radius)	°	32
Scintillator thickness	mm	7
Gap thickness	mm	8.5
Size of tower at outer radius (approximate)	mm	132
Sampling fraction at inner radius		0.078
Sampling fraction at outer radius		0.060

Table 5: Design parameters for the inner Hadronic Calorimeter Prototype.

direction as seen from the interaction point). In each run 4 vertical towers are scanned from top to bottom (e.g. Tower 0-3 in Figure 13). This
295 yields 8 individual runs in order to fully calibrate both the inner and outer HCal. Figure 13 shows the ADC distributions in the 4×4 inner HCal towers. Each spectrum is fitted with an exponential+Landau function, where the exponential function corresponds to the background and the Landau function represents the MIP events. As seen in the figure, the background
300 component is relatively small. Clear cosmic MIP peaks are observed in all towers.

The corresponding simulation of cosmic muons are performed at 4 GeV (the mean muon energy at sea level) at the top of the HCal prototype moving downwards with our standard GEANT4 setup. The mean energy deposited by the cosmic muons in each tower is ≈ 8 MeV for the inner HCal. Because of the tilted plate design, towers at the bottom of the inner HCal have more deposited energy than the top ones. This feature was first observed in data and then confirmed by the simulations. We used this simulation to calibrate

Parameter	Units	Value
Inner radius (envelope)	mm	1820
Outer radius (envelope)	mm	2685
Length (envelope)	mm	??
Material	1006 magnet steel	
Number of towers in azimuth ($\Delta\phi$)		4
Number of tiles per tower		5
Number of towers in pseudorapidity ($\Delta\eta$)		4
Number of electronic channels (towers)		16
Module weight (estimated)	kg	900
Absorber plate thickness at inner radius	mm	10.2
Absorber plate thickness at outer radius	mm	14.7
Total number of absorber plates		21
Tilt angle (relative to radius)	°	12
Scintillator thickness	mm	7
Gap thickness	mm	8.5
Size of tower at outer radius (approximate)	mm	132
Sampling fraction at inner radius		0.037
Sampling fraction at outer radius		0.028

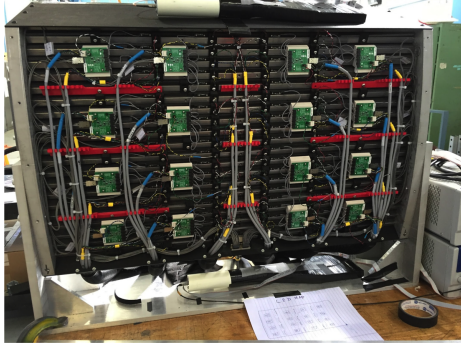
Table 6: Design parameters for the outer Hadronic Calorimeter Prototype.

the ADC signal in each tower to the corresponding energy loss in the test beam. Once the ADC signal height $I(ch)$ is determined by a functional fit to the ADC timing samples, the energy deposited is calculated by:

$$E(ch) = I(ch) \frac{E_{dep}^{cosmic}(ch)}{E_{dep}^{ADC}(ch) \times SF(muon)}, \quad (1)$$

where $E_{dep}^{cosmic}(ch)$ is the total deposited energy extracted from the GEANT4 simulations, $E_{dep}^{ADC}(ch)$ is the ADC signal height measured from cosmic data, and $SF(muon)$ is the muon sampling fraction.

305 In addition to the cosmic calibration, an LED pulser calibration system is incorporated in the HCal. It monitors short term gain changes caused by temperature changes and increased leakage current caused by radiation damage.



(a)



(b)

Figure 12: Fully assembled (a) inner and (b) outer section of HCal.

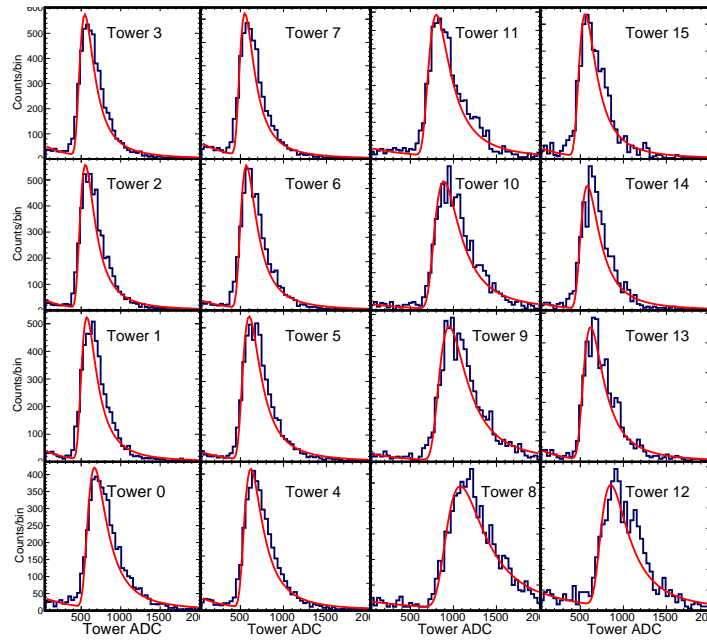


Figure 13: ADC spectrum of cosmic MIP events in the inner HCal.

4. Readout Electronics and Data Acquisition

310 4.1. Overview

A common electronics design has been chosen for the readout of the sPHENIX EMCal and HCal detectors using commercially available components. This approach reduces the overall cost and minimizes the technical risks associated the detector electronics. The design uses multiple Silicon
315 Photomultipliers (SiPMs) from Hamamatsu as the optical sensors to read out the calorimeters. Signals from the SiPMs associated with a calorimeter tower are passively summed, amplified, shaped, and differentially driven to a digitizer system located near the detector. The signals are continuously digitized at 60 MHz and delayed in a digital pipeline pending a Level-1
320 trigger from the trigger system. Upon receipt of a Level-1 trigger, the data for 16 time slices corresponding to the triggered event for all towers in the EMCal and HCal are recorded for analysis. In addition to the calorimeters, signals from the beam line Cherenkov counters and finger hodoscopes are recorded. Details of the readout electronics for the calorimeters are
325 discussed in the following sections.

4.2. Optical Sensors

The compact nature of the EMCal and HCal detectors and the location of the EMCal and inner HCal being inside the 1.5T solenoidal field of the sPHENIX detector require that the optical sensors be both physically small
330 and immune to magnetic effects. A device with large gain is also desirable in order to reduce the demands on the performance specifications of the front end analog electronics. SiPMs have the advantage that there are immune to magnetic fields, have large gain and are small in size. For both the electromagnetic and hadronic calorimeters, the Hamamatsu S12572-33-
335 015P MultiPixel Photon Counters (MPPC) has been selected as the optical sensor. The device has a light collection area of $3 \times 3 \text{ mm}^2$ with 40K pixels each $15 \times 15 \mu\text{m}^2$ in size. The properties of this device are summarized in Table 7.

The gain of an SiPM is very sensitive to the temperature, which can be
340 corrected for. In order to account for runs taken with different temperatures we took runs to calibrate the temperature correction. Figure 14 shows the calibrated signal (in GeV) vs the average (event-by-event) temperature across the 5x5 region in the EMCAL around tower 21. Note that the temperature may be offset by some constant due to lack of calibration. Data

Property	Value
Active area	3mm x 3mm
Number of micropixels	40,000
Micropixel pitch	15 μm
Geometric fill factor	0.53
Package	surface mount
Window	epoxy resin
Window refractive index	1.55
Operating temperature	0-40 deg C
Spectral response range	320-900 nm
Peak sensitivity wavelength	460 nm
Photon detection efficiency (PDE)	0.25
Dark count rate (typ)	1 Mcps
Terminal capacitance	320 pF
Gain	230,000
Gain temp coefficient	3500 / $^{\circ}\text{C}$
Breakdown voltage (V_{br})	$65 \pm 10 \text{ V}$
Recommended operating voltage	$V_{\text{br}} + 4\text{V}$
Temp coeffic at V_{op}	60 mV / $^{\circ}\text{C}$

Table 7: Properties of Hamamatsu S12572-015P MPPC.

is taken in two conditions, with the blower open and closed to give different temperature ranges and a temperature compensation is determined and applied to correct the data. Figure 14 (a) shows data without temperature compensation applied, relative to a 16 GeV beam. This corresponds to about $-3.68 \pm 0.29\%/^{\circ}\text{C}$. Figure 14 (b) shows data with temperature compensation applied, relative to a -16 GeV beam. This corresponds to about $1.30\%/^{\circ}\text{C}$. All data shown is recorded for single temperature and assumes no uncertainty in temperature.

4.3. Analog Front End

The preamps used to amplify SiPM signals from both the EMCal and HCal portions of the detector are the same, differing only in packaging. The signals from the SiPMs associated with a calorimeter tower are passively summed and then amplified. The amplifier front end is a common-base configuration acting like a transresistance amplifier or “current conveyor”. This configuration presents a very low impedance to the SiPMs thereby minimizing any voltage swing on the device. A charge injection circuit is

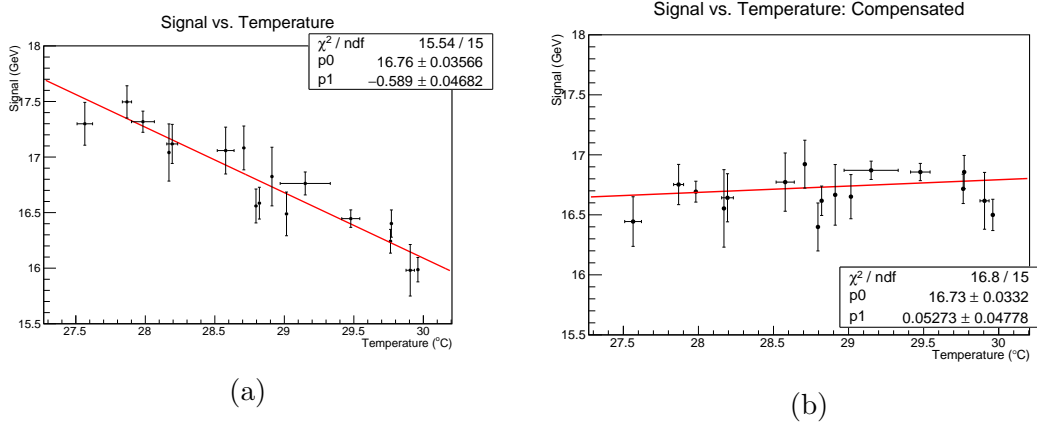


Figure 14: (a) Signal vs. Temperature without temperature compensation, and (b) Signal vs. Temperature with temperature compensation

included to generate a fixed test pulse to the amplifier. The signal then passes through gain circuitry which can select either normal gain or a high gain range of 32X normal for the purpose of discerning single photoelectron events for a direct gain measurement. The signal is then shaped with a peaking time of 30 ns for 60 MHz sampling and driven differentially to the external ADC electronics.

The EMCAL preamplifier module consists of eight preamp channels with 4 SiPMs per channel laid out to match the tower geometry of a 1x8 EMCAL block. A small surface mount thermistor is centered between the 4 SiPMs in a tower to monitor the local temperature of SiPMs. Located on the edge of the preamplifier module centered between pairs of EMCAL towers are 4 LEDs that are used for monitoring and testing. Pictures of the front and back of a partially assembled EMCAL preamplifier module are shown in Figure 15. The SiPMs for the HCal are mounted on small daughter boards that are directly attached to the tiles forming an HCal tower. The SiPM daughter boards are connected to an HCal preamp board located on the detector with a short twisted pair cable. An LED is also positioned near each SiPM for monitoring and testing. A thermistor is located near one of the SiPMs in each tower to monitor the local ambient temperature.

4.4. Slow Control

A slow control system is necessary to provide stable and controllable operational parameters for the SiPMs. The sPHENIX Slow Controls are organized in a tree structure to facilitate the monitoring and control of

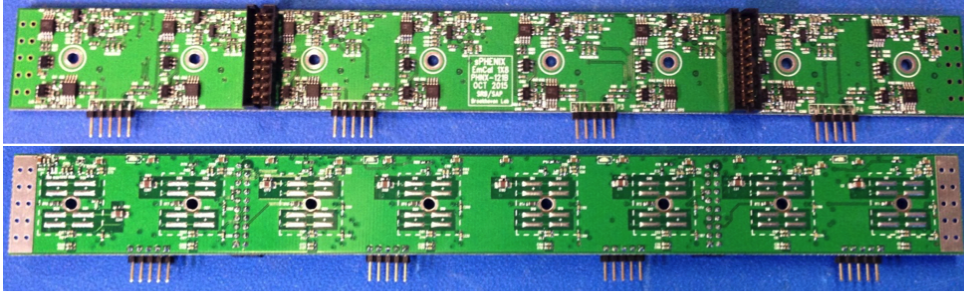


Figure 15: An EMCAL 1x8 preamp board (top and bottom). The top side contains all the analog circuitry. The SiPMs mount on the pads on the bottom of the board.

a large number of channels in the final detector configuration. The Slow Controls system provides:

- Channel bias control
- SiPM leakage current readback
- SiPM temperature measurement
- Input voltage and voltage regulator temperature
- Pulse control for both charge injection and LED test pulse
- SiPM temperature and leakage current compensation.

The Slow Controls system is comprises an Interface board and Controller board. The Interface board, located on the detector, contains ADCs for monitoring temperatures, voltages, and leakage current, and DACs for adjusting the SiPM bias voltage. In addition, the Interface board provides power and bias distribution to the preamp boards. For both the EMCAL and HCal the Interface Board functionality is the same; however, the packaging is different to account for difference in geometrical constraints of the two systems. The Interface board is connected via a bi-directional serial link to a Controller board in a nearby crate. The Controller board transmits to the Interface board the parameters for gain control, temperature compensation, LED enables, and pulse triggers, and reads back monitoring information. Communication with the Controller board is ethernet based. The same Controller Board is used for both systems. A schematic overview of the slow control system is shown in Figure 16.

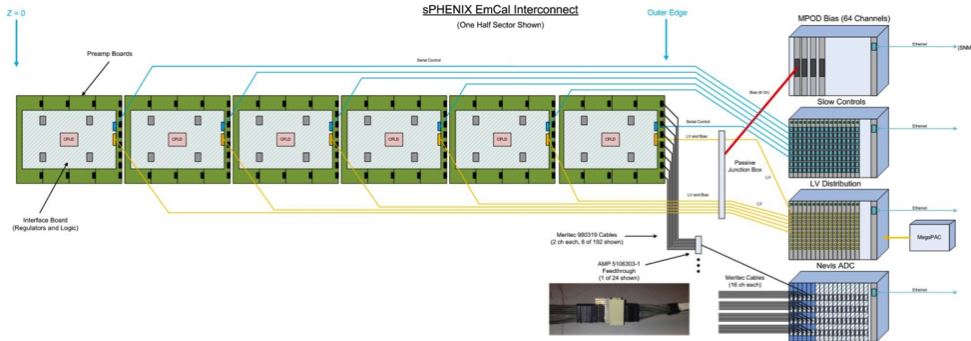


Figure 16: Schematic overview of the slow control system for the EMCal and HCal.

The Controller boards are 6U Ethernet Telnet servers housed in external racks that control the Interface boards via isolated RS-485 serial lines over standard CAT5 cables. In addition to providing a monitor and control portal, the Controller processes temperature and leakage current values to provide individual SiPM temperature and leakage current compensation if so commanded. Two Controllers are used for the T-1044 Beam Test, one for EMCal and one for HCal. A single EMCal Interface board serviced the 64 channel EMCal apparatus. A separate HCal Interface board is used for each of the 16 channel Inner and Outer arms.

4.5. LED Monitoring

To provide monitoring and testing of the calorimeter electronics, an LED pulser system is used. For the EMCal, four 405nm LEDs are placed on the preamp board such that they are centered between 4 EMCal towers, 2 towers associated with the preamp board and 2 towers associated with the neighboring preamp board. The LEDs are driven with a fixed amplitude pulse. For the HCal, a 405nm LED is embedded in the edge of each of the five tiles associated with an HCal tower. The LEDs could be pulsed individually with using a programmable driver circuit.

4.6. Digitizers

The analog signals from the front end amplifiers are transmitted differentially over a 10 m Hard Metrics 16 channel signal cable to a custom digitizing system originally developed for the PHENIX Hadron Blind Detector (HBD) [13] and modified to operate with the PHENIX Muon Piston Calorimeter (MPC) and Resistive Plate Chamber (RPC) detectors. The

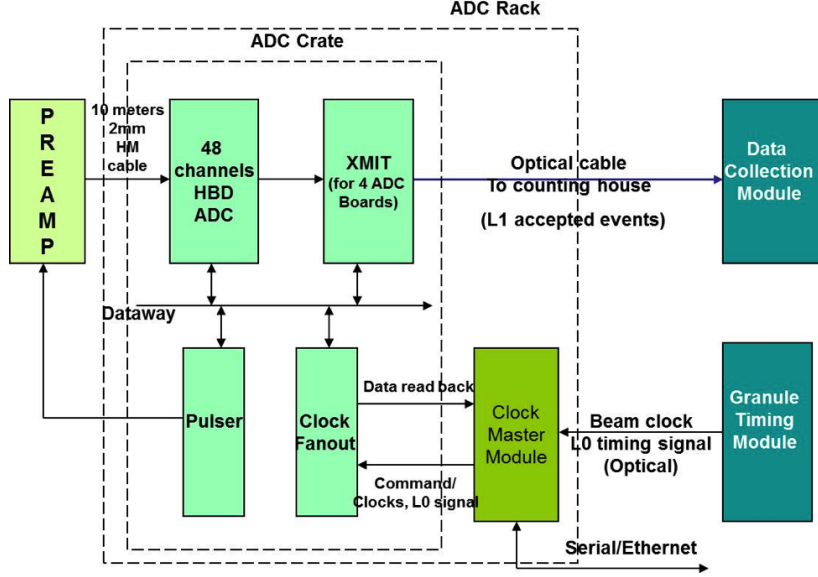


Figure 17: Block diagram of the HBD digitizer system used for the readout of the prototype calorimeters. For the test beam running an internal 60 MHz clock is used.

430 overall layout of the digitizer system interface to the DAQ system is shown in Figure 17. The signals are received differentially and digitized by a 12 bit flash ADC running at a 60 MHz sampling frequency. The output of the ADC is transmitted to a local FPGA which provides a 4 μ s pipeline delay for buffering events for a Level-1 trigger. Upon receipt of a Level-1
 435 trigger, the ADC data for the 16 time samples is transmitted via optical fiber to a PHENIX Data Collection Module (DCM). The formatted data is transmitted to a local computer for logging to disk. The system is design to operate at a maximum data rate of 15kHz.

4.7. The Data Acquisition System

440 The current data acquisition system in use for most R&D-level efforts is called RCDAQ [14]. The data written by RCDAQ are format-compatible with the main PHENIX and sPHENIX data acquisition system, so all analysis code developed in the course of the R&D efforts can be re-used at a later stage.

445 RCDAQ has a number of features which are indispensable in a test beam setting. It is client-server based, and can be controlled from multiple clients. There is no “central console” for the operation of the DAQ system. This

allows, for example, to start the DAQ from the beam enclosure while an access is underway to verify the proper state of all components before ending the access.

RCDAQ allows to capture any kind of ancillary data that can be accessed from the DAQ computer, such as temperature readings, voltage levels, and camera pictures. Those are embedded in the primary data stream and cannot be separated from the data and therefore cannot get lost.

During the 2016 test beam, we recorded, in addition to the ADC values from the calorimeters and beamline detectors, 57 additional pieces of information, among them 3 different camera pictures, temperature information for all SiPMs, bias voltages, gain settings, positioning table coordinates, etc. The additional information captured provides everything that is needed during the eventual analysis of the data, eliminating the need to consult a logbook (with potentially erroneous entries) for that information. The data captured is comprehensive enough to allow a “forensics-type” investigation of one finds that some result is questionable for some reason.

The primary information the RCDAQ system reads are the signals from the SiPMs of the calorimeter towers. The same ADC system also reads out a number of beamline instrumentation detectors, such as threshold Cherenkov detectors that allow to distinguish between different particle species, a beam hodoscope, and the like.

RCDAQ offers an online monitoring stream, which provides the most recent data on a best-effort basis (the online monitoring is not allowed to raise the DAQ busy and throttle the data rate). This monitoring allows to recognize tripped voltage supplies, noise, of dead channels in a timely manner.

5. Test Beam

Testing of the prototype detectors was performed at the Fermilab Test Beam Facility (FTBF) under the T-1044 experiment. The facility has two beamlines which can produce a variety of particle types over a range of energies up to 120 GeV. The T-1044 experiment used the MTest beamline which has two modes of operation; primary protons at 120 GeV and a secondary mixed beam consisting primarily of pions, electrons and muons with energies ranging from 1 to 60 GeV of either positive or negative charge. The beam energies used for T-1044 were secondary beams of 2, 4, 6, 8, 12, 16, 20, 24, and 32 GeV, and primary protons at 120 GeV. The beam is delivered as a slow spill with a 4 sec duration once per minute with a

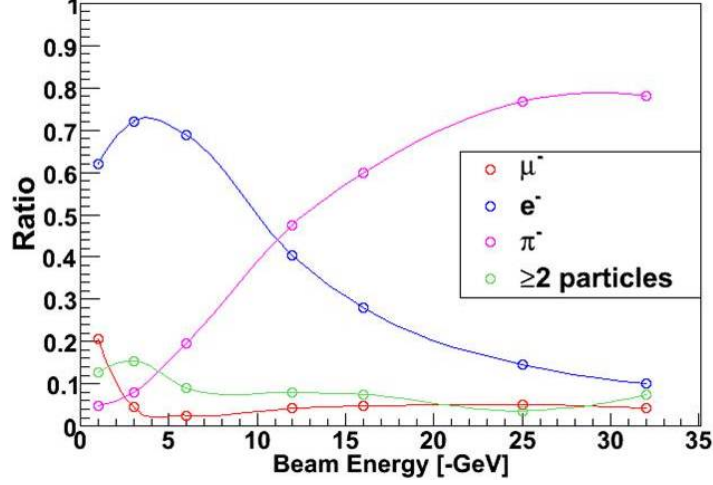


Figure 18: FTBF negative polarity beam profile

485 maximum intensity of a $\sim 10^5$ particles per spill. The momentum spread of the beam depends on the beam tune and is $\sim 3\%$. The beam spot size is also dependent on the beam energy and tune and ranges from $\sim 6\text{mm}$ to several centimeters in size. The secondary beam composition is plotted in Figure 18 showing the relative contribution of electrons, muons and hadrons present in the beam as a function of energy [15, 16]. The kaon content in the beam is expected to be around 1% between 20-32 GeV/c [17].

490 The FTBF also provides a number of detectors for test beam groups to use. These include 2 differential Cherenkov counters upstream of the MTest enclosures, lead glass with PMT, multi-wire proportional chambers (MWPC) and trigger counters. Full details of the facility can be found in on the FTBF website [15].

500 The MTest beam line has several areas that can be used and for T-1044 the MT6.2C and MT6.2D areas were utilized. For the initial tests of the EMCal, the EMCal detector was placed on the MT6.2C motion table. The motion table allowed the detector to be moved horizontally with respect to the beam remotely allowing for detailed scan of the detector. For the second half of running, the EMCal was moved to a rail systems directly in front of the Inner HCal allowing for combined EMCal/HCal testing.

505 Due to its size, the HCal was positioned in the MT6.2D area on the floor. The support table allowed the HCal to be adjusted in the vertical direction. A total tilt angle of $\pm 5^\circ$ was possible. In order to simulate

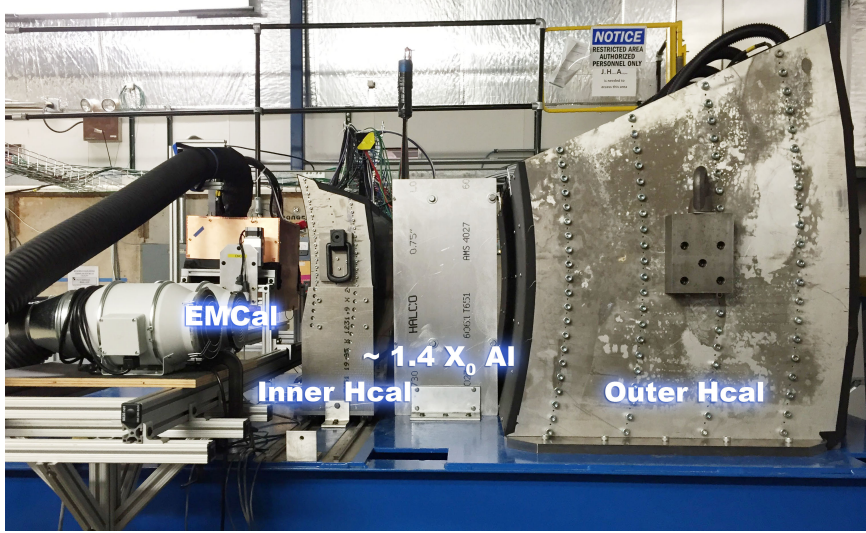


Figure 19: T-1044 Testbeam setup

the effects of the sPHENIX solenoid, a “mock” cryostat was constructed from Aluminum plates with the same thickness and radiation length as the sPHENIX solenoid. Figure 19 shows a picture of the of the prototype setup in the MT6.2D area.

A hodoscope and veto counters were installed upstream of the EMCal to allow for the selection of beam particles impinging on the EMCal detector. The hodoscope consists of sixteen 5 mm finger counters (8 vertical, 8 horizontal) readout with SiPMs. The signals from the SiPMs were amplified, shaped, and readout using the HBD digitizers. Four scintillator counters surrounded the hodoscope and are readout using PMTs and digitized using the HBD digitizers.

A Pb-glass calorimeter was used to calibrate the test beam. It is known to have a nominal energy resolution of $6\%/\sqrt{E}$ (GeV), [18]. We measured the energy resolution at two different voltages 1100V and 1200V and obtained the result of $2.4\% \oplus 5.69\%/\sqrt{E}$, see Figure 21

6. Simulations

We have employed the GEANT4 simulation toolkit [19] for our full prototype device simulations. It provides collections of physics processes suitable for different applications. We selected the QGSP_BERT_HP list as the default, which is recommended for high energy detector simulations like the

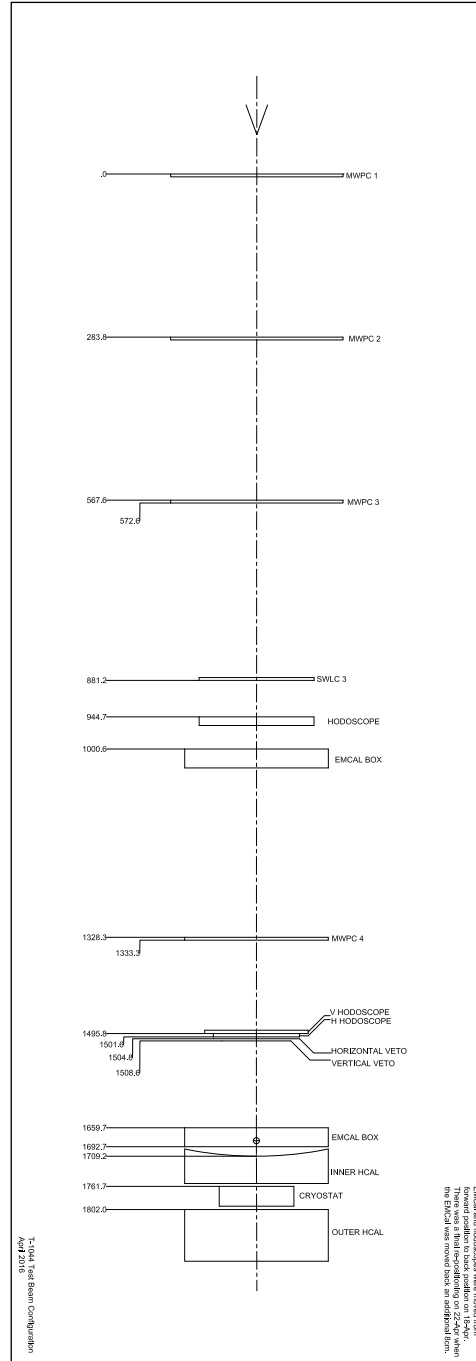


Figure 20: Beam line setup.

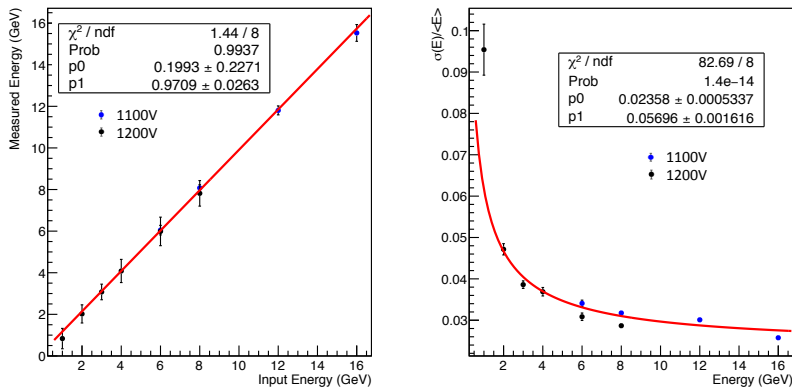


Figure 21: Pb Glass energy resolution at 1100V and 1200V.

LHC experiments. We have also run additional tests with different physics lists in detailed comparison with test beam results. All tracks which reach a layer 10 cm behind the HCal or outside the calorimeter region on the sides are aborted to count for shower energy leakage.

We have integrated the sPHENIX simulations with the sPHENIX software framework [20], enabling us to use same analysis software to analyze both simulated and test beam data. In Section 5, the simulated detector performance data are compared with the real data, which demonstrates an accurate description of the detector performance in simulation.

The EMCal has been simulated using the GEANT4 tools described above. A detailed description of the 8×8 SPACAL towers as constructed for the test beam is implemented. Figure 22 shows a typical GEANT4 event in which a 8 GeV/c electron showers the EMCal.

The HCal includes the detailed geometry of the steel plates and interleaved scintillator tiles. Between the inner and outer HCals, three aluminum plates are inserted as in the construction of the prototype device, to represent the material distribution inside the BaBar magnet and cryostat. Their location and thickness are also assigned according to the actual test beam device. Figure 23 shows a typical GEANT4 event in which a 30 GeV/c π^- incident on the calorimeter showers in the full prototype device.

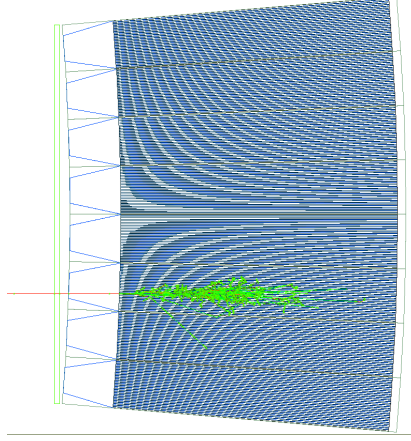


Figure 22: Side view of an 8 GeV electron shower as simulated in the EMCAL prototype. The incoming electron (red line on the left edge) passes through the light guide (blue trapezoid) and develops an EM shower in the EMCAL blocks that consist of W-epoxy absorber (invisible) and scintillation fibers (blue stripes). A 1/10-inch-thick G10 sheet is placed before EMCAL to represent the average thickness of the electronics and cooling assembly.

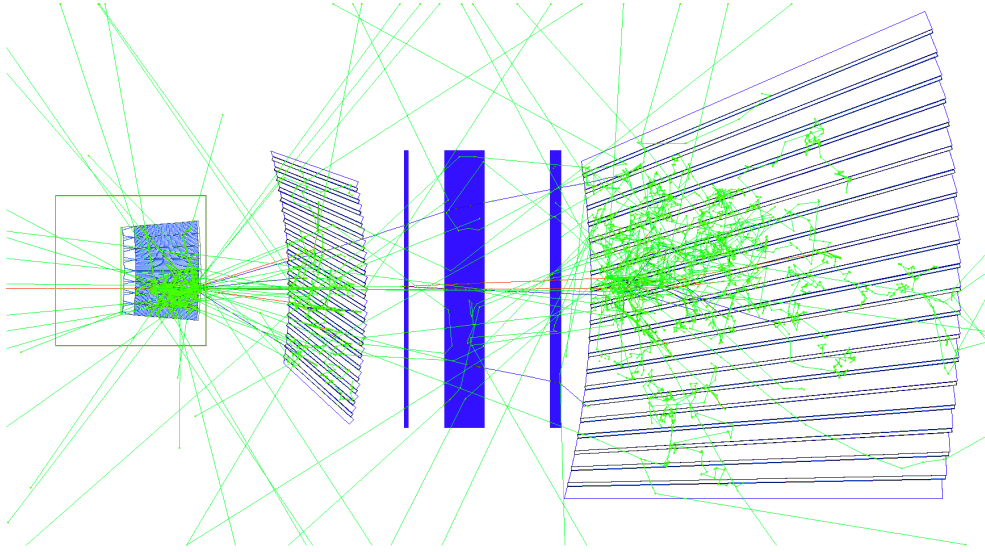


Figure 23: Side view of 32 GeV π^- shower as simulated in the EMCAL and HCal prototype. The incoming pion (red line on the left edge) starts to develop a shower in the EMCAL (left box), which is further absorbed in the inner HCal (tilted plates in the middle), three aluminum plates as a mock up of the BaBar magnet (blue block) and the outer HCal (tilted plates on the right side).

After the GEANT4 simulation stage, several steps are implemented to simulate for the ADC response in the tower:

1. Energy depositions for each GEANT4 tracklet in the scintillation volume are collected in the sPHENIX analysis framework.
2. The Birks' law of scintillator non-linearity [21] with a default Birks' constant of $k_B = 0.0794$ mm/MeV [22] is implemented to convert ionizing energy deposition to visible energy that is proportional to the expected number of photons produced in the scintillator.
3. The visible energy in each calorimeter tower is summed in a timing window of 0-60 ns to calculate the mean number of active pixels in the SiPM readout. In the case of the EMCal, the sum of visible energy is also modulated by the position of scintillation light production, which accounts for the measured attenuation in the scintillation fiber and the non-uniformity in the light collection efficiency for the light guide as shown in Figure 4. The scale of the mean number of active pixels is set by the mean active pixel count as measured in cosmic tests of the EMCal and HCal. The actual active pixel number is a random number following a Poisson distribution with a parameter of the mean number of active pixels.
4. In the last step, the ADC for each readout channel is proportional to the sum of the actual active pixel number and a random number following the pedestal distribution. The sum is scaled to an ADC value using measured pixel/ADC value from cosmic tests and discretized to integers of ADC value.

Under the sPHENIX software framework [20], analysis software picks up the simulated ADC value, and process it in a consistent way as that for the test beam data, including an energy scale calibration, clusterizing and producing performance plots. The results for simulation and test beam data are compared in Section 5.

7. Results

The results from the test beam T-1044 at Fermilab are studied for three different configurations. First the EMCal is tested as a standalone calorimeter, then the inner and outer HCal are tested, and finally both calorimeters are tested together to produce joint data. The presented analysis is based on the data collected with the negatively charged particle beams from 1 GeV to 64 GeV.

The experimental setup is described in 5. Two differential gaseous Cherenkov counters are placed upstream of the calorimeter setup and used
585 for offline discrimination between pions and electrons on an event-by-event basis. The gas pressures of the counters are set between the pion and electron thresholds. The inefficiency of the Cherenkov counters resulted in only a few percent of contamination for both the electron and pion samples.

There are four veto counters arranged around the beam with one above,
590 one below, one to the left and one to the right of the beam. If any one of the veto counters measures energy above a certain threshold, the event is rejected due to the position of the beam.

In addition there are two sets of hodoscope fingers, one set of eight fingers arranged vertically, and other set of eight fingers arranged horizontally.
595 Each hodoscope finger is 5 mm in width and made from a plastic scintillator read out by a PMT. As shown in Figure 18, a small fraction of events have more than 2 particles in one event. In order to remove those events we require that each event has only one valid horizontal and vertical hit.

7.1. *EMCal*

600 For the MIP calibration runs, the EMCal is rotated downward from its nominal position, and then rotated 180 degrees with respect to the axis perpendicular to the beam. The beam is centered on one column per run, such that the beam passes through all 8 towers in a column. Events used for the MIP calibration are required to have counts above the pedestal for
605 each tower in the column of interest and no counts above pedestal for all other towers. The ADC spectrum for each tower is fitted with a Gaussian+Landau function over the region above pedestal. The MIP peaks in Figure 24 correspond to the ADC value at the maximum of the fit.

An upper limit on the Cherenkov background, produced when charged
610 particles pass through the acrylic light guides, is estimated using dedicated runs in the test beam. With the EMCal towers rotated perpendicular to the incoming beam, 120 GeV/c protons are set to pass through a column of light guides or a column of SPACAL towers. Events in which a proton initiates a hadronic shower are rejected by vetoing events with non-zero energy in
615 the EMCal towers other than the column being studied. The mean energy from the Cherenkov background when the proton beam MIPs through the light guide is found to be less than 11% (90% C.L.) of the MIP energy when a proton passes perpendicularly through the EMCal towers, as shown in Figure 25 and Figure 26. Since in the nominal orientation of the EMCal,
620 the incoming particle travels away from the photon sensor, the Cherenkov

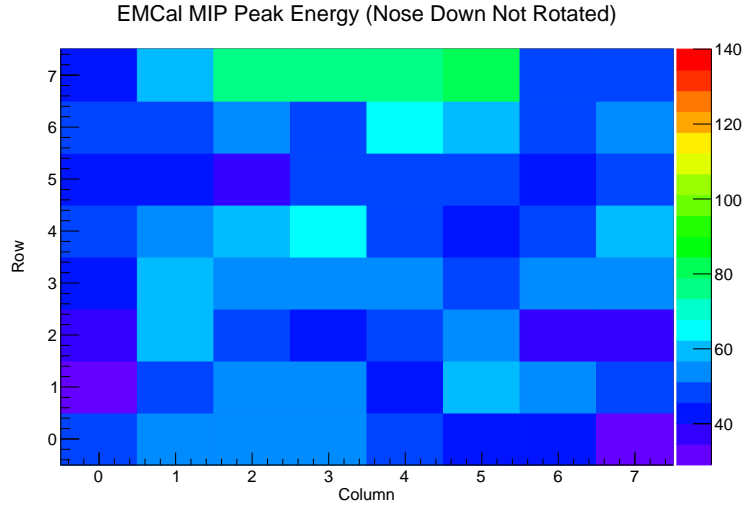


Figure 24: EMCal MIP Peak Energy with the nose rotated down by 180 degrees.

background during physics data taking is expected be significantly smaller than this estimated upper limit.

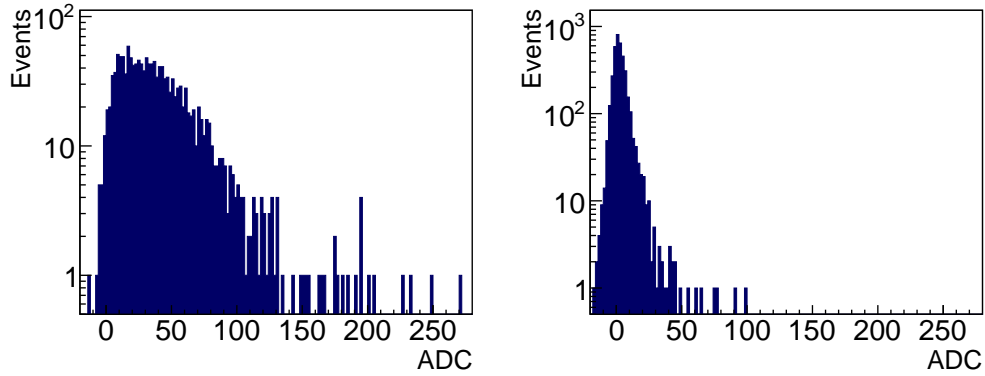


Figure 25: Typical ADC distribution for MIP energy when the 120 GeV/c proton beam passes perpendicular through an EMCal tower (left), and when it pass through a light guide via its sides (right). (Editorial comment: This could be too detailed for this paper. Suggestion welcomed.)

The EM energy resolution for the EMCal is obtained using the electron component of the test beam, which is selected using the Cherenkov detectors, tuned to produce a signal for electron events, but not for hardrons and muons. However, due to multiple particle events as discussed in Section 5,

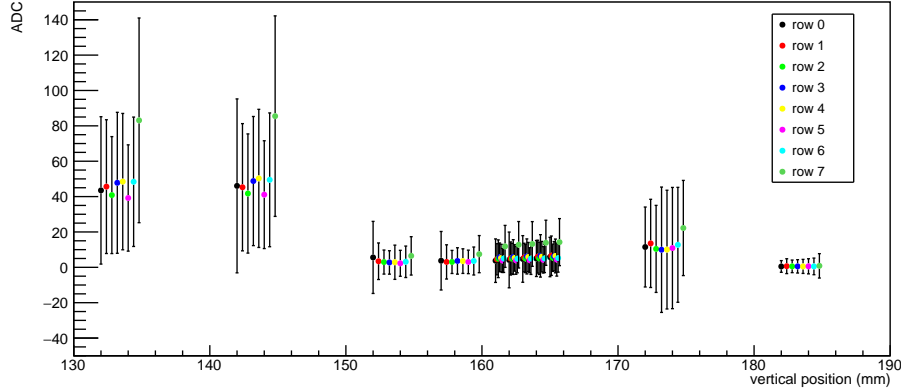


Figure 26: The mean and RMS of the ADC distribution plotted against the vertical lift position of the EMCAL prototype. The EMCAL towers are rotated perpendicular to the incoming 120 GeV/c proton beam. The beam spot after a hodoscope cut is less than $5 \times 5 \text{ mm}^2$. At vertical lift position less than 150 mm, the beam passes through the SPACAL blocks, where the MIP energy is extracted; between a position of 150-170 mm, the beam passes through the light guide, where the Cherenkov photon background is measured; at around 172 mm, beam is centered on the SiPMs; for positions higher than 180 mm, the beam passes cleanly below the photon sensors. (Editorial comment: This could be too detailed for this paper. Suggestion welcomed.)

the lower energy electron events still contains a fraction of hardron and muons, which are further rejected using the EMCAL energy response. For each event, calibrated EMCAL tower energy is summed within a 5×5 tower cluster centered around the max-energy tower, which is histogrammed in Figure 27. The mean energy and spread of EMCAL response at each beam energy is extracted with a Gauss fit at the electron peak prior to unfolding a beam momentum spread ($\Delta p/p \approx 2\%$). The mean and ratio between standard deviation and mean from each fit are plotted against the beam energy as linearity and resolution as shown in Figures 28, 29, and 31. Two types of electron resolution are studied:

- Resolution for showers located at the center of one tower, which is a test of the intrinsic performance of the W-Epoxy and fiber sampling structure with minimal sensitivity to the light collection uniformity and tower edge effects. With a $10 \times 5 \text{ mm}^2$ beam hodoscope selection around the center of one tower, the linearity and resolution are shown in Figure 28 and 29 for SPACAL towers produced at UIUC and THP, respectively. At a 10 degree incident angle, the perfor-

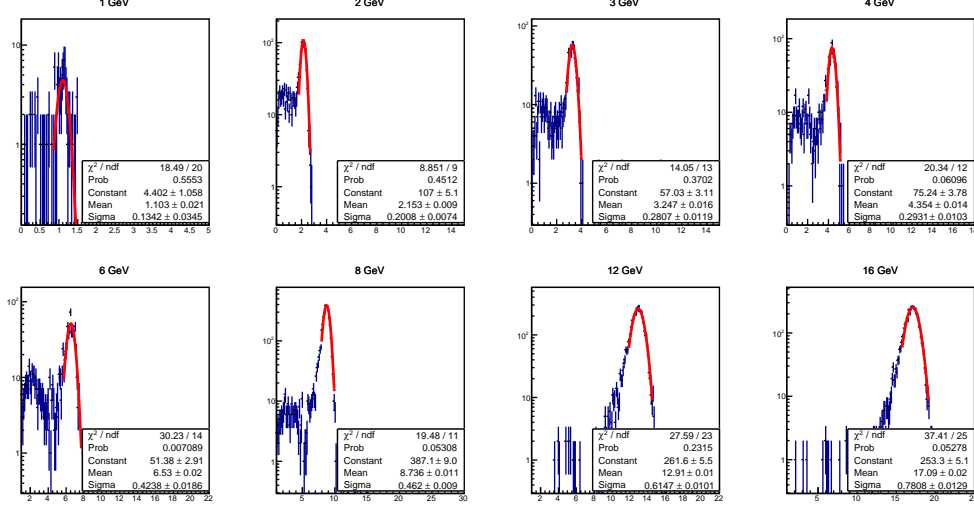


Figure 27: Cluster energy distribution of electron showers in EMCal (blue points), for which the beam incident angle is 10 degrees and a $5 \times 5 \text{ mm}^2$ beam cross section is selected at the center of one EMCal tower. The central tower and most near-by tower are produced at UIUC. For each panel, data for one choice of beam energy is selected as shown in the title and the energy resolution prior to unfolding a beam momentum spread ($\Delta p/p \approx 2\%$) is extracted with a Gauss fit at the electron peak (red curve). Low energy tails stems from multi-particle background is excluded from the fit.

mance of the UIUC and THP SPACAL towers are comparable with each other and with that of simulation, producing a resolution of $\Delta E/E = 2.6\% \oplus 12.3\%/\sqrt{E}$ after unfolding the beam momentum spread. At a 45 degree beam incident angle, the resolution is found to be $\Delta E/E = 0.9\% \oplus 14.9\%/\sqrt{E}$ after unfolding the beam momentum spread.

- Resolution without restriction of beam position, which is more relevant for performance projection in sPHENIX. The energy response of the EMCal depends on the hit position of the incoming particle, which mainly stems from the non-uniformity of light collection on the light guide as illustrated in Figure 4. While the next stage of EMCal R&D emphasizes on improving light collection uniformity, a position dependent energy scale correction is applied to the current data based on the two-dimensional beam position as measured using a $5 \times 5 \text{ mm}^2$ hodoscope selection. Figure 30 shows the performance of position correction for a sum of all events within a $25 \times 25 \text{ mm}^2$ beam cross that

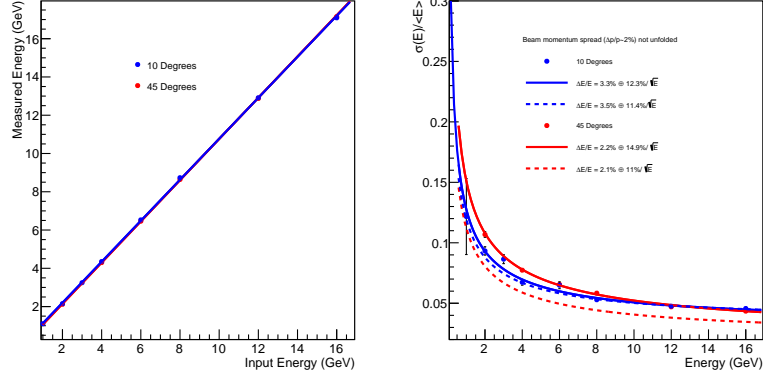


Figure 28: Linearity and resolution of electron showers in EMCAL towers produced at UIUC, for which a $10 \times 5 \text{ mm}^2$ beam cross section is selected at the center of one EMCAL tower. The beam incident angles are 10 degrees (blue) and 45 degrees (red). Data (points) are fit with linear (left solid curves) and $\Delta E/E = \sqrt{a^2 + b^2/E}$ function with results labeled on plot (right solid curves), which are compared with simulation (dashed curves). A beam momentum spread ($\Delta p/p \approx 2\%$) is *not* unfolded and included in the resolution.

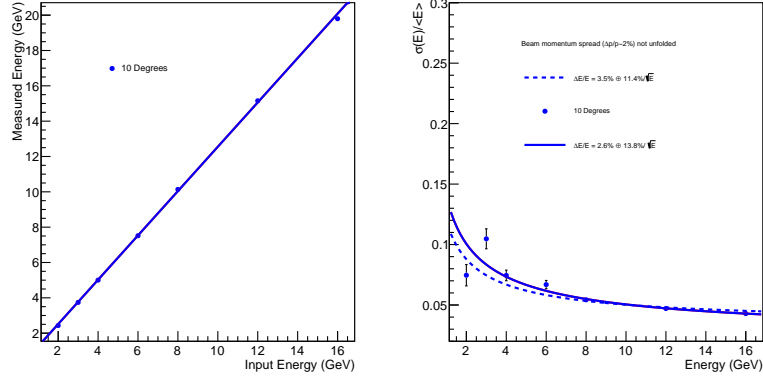


Figure 29: Linearity and resolution of electron showers in EMCAL towers produced at THP, for which a $10 \times 5 \text{ mm}^2$ beam cross section is selected at the center of one EMCAL tower. Legend is the same to Figure 28.

660

matches the full cross section of one SPACAL tower before and after the correction is applied. Figures 31 and 32 show the result after this correction is applied to the for SPACAL towers produced at UIUC and THP, respectively. The EMCAL resolution after unfolding the beam

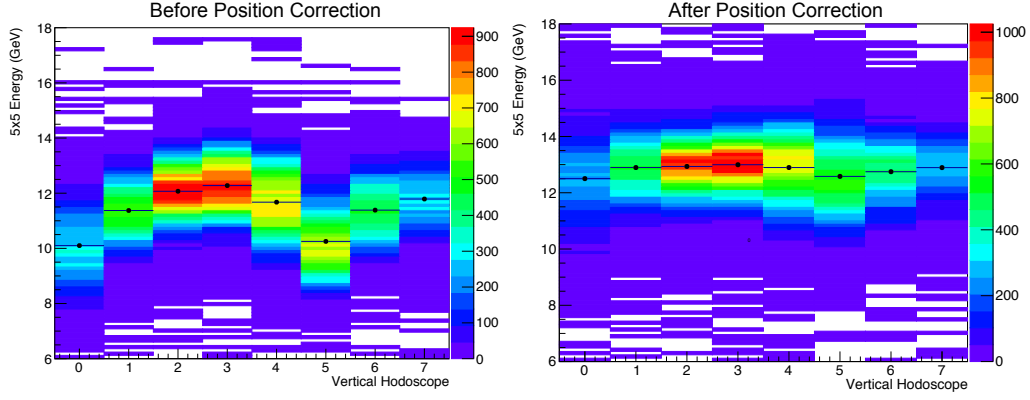


Figure 30: Cluster energy vs. vertical hodoscope in the EMCal towers produced at UIUC before and after the position correction for a $25 \times 25 \text{ mm}^2$ beam cross section is applied. The beam energy shown is at 12 GeV with an incident angle of 10 degrees. Data is shown prior to unfolding a beam momentum spread ($\Delta p/p \approx 2\%$).

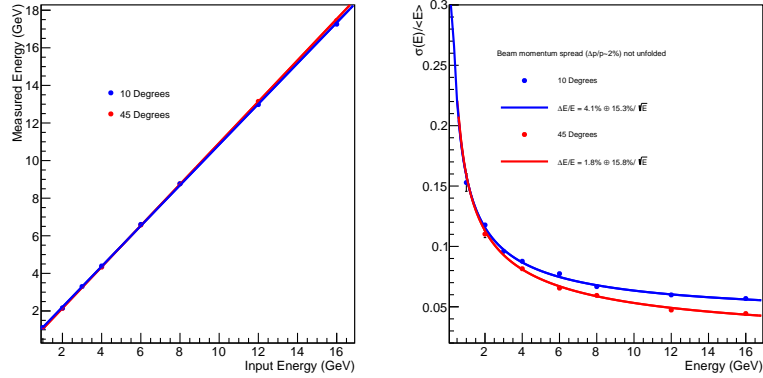


Figure 31: Linearity and resolution of electron showers in EMCal towers produced at UIUC, for which a $25 \times 25 \text{ mm}^2$ beam cross section is selected and matches the area of one EMCal tower. The beam incident angles are 10 degrees (blue) and 45 degrees (red). Data (points) are fit with linear (left solid curves) and $\Delta E/E = \sqrt{a^2 + b^2/E}$ function with results labeled on plot (right solid curves). A beam momentum spread ($\Delta p/p \approx 2\%$) is NOT unfolded and included in the resolution.

momentum spread is $\Delta E/E = 3.6\% \oplus 15.3\%/\sqrt{E}$ at a 10 degree beam incident angle and $\Delta E/E = 15.8\%/\sqrt{E}$ (with a negligible constant term) at a 45 degree beam incident angle.

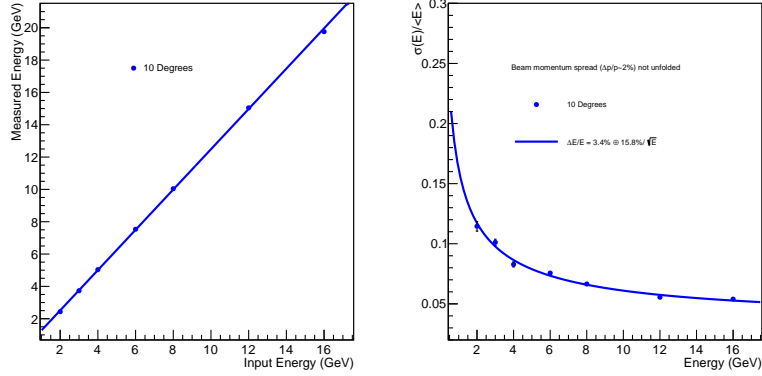


Figure 32: Linearity and resolution of electron showers in EMCal towers produced at THP, for which a $25 \times 25 \text{ mm}^2$ beam cross section is selected and matches the area of one EMCal tower. Legend is the same to Figure 31.

An important function of the EMCal in sPHENIX is to provide electron identification and hadron rejection for charged tracks via a minimal E/p cut. As shown in Figure 33, the hadronic component of the test beam is selected to quantify the hadron rejection in the prototype, which are compared with various simulation tunes of GEANT4 physics lists [19] and Birks' constant for scintillator non-linearity [21]. The hadronic shower events are selected by requiring no activity in the beam-line Cherenkov detectors, which are tuned to produce Cherenkov signals on electrons but not on hadrons. Then based on Figure 18, the expected muon component in the beam is simulated and statistically subtracted from the cluster energy spectrum. The resulting EMCal cluster energy spectrum contains mainly π^- events, which are converted to rejection versus minimal cluster energy cut as in Figure 33. The kaon content is expected to be very small, about 1% of beam content at higher momenta (20-30 GeV/c [17]), and lower at lower momenta (4-12 GeV/c) due to the decay of kaons in flight. Both π^- and K^- are simulated and compared with the data. All simulation tunes reproduce the rejection for rare high energy hadronic showers in EMCal within a factor of two. Meanwhile, the simulation tune using QGSP_BERT_HP physics list [19] with $k_B = 0.18 \text{ mm/MeV}$ [23] is the most consistent with the test beam data.

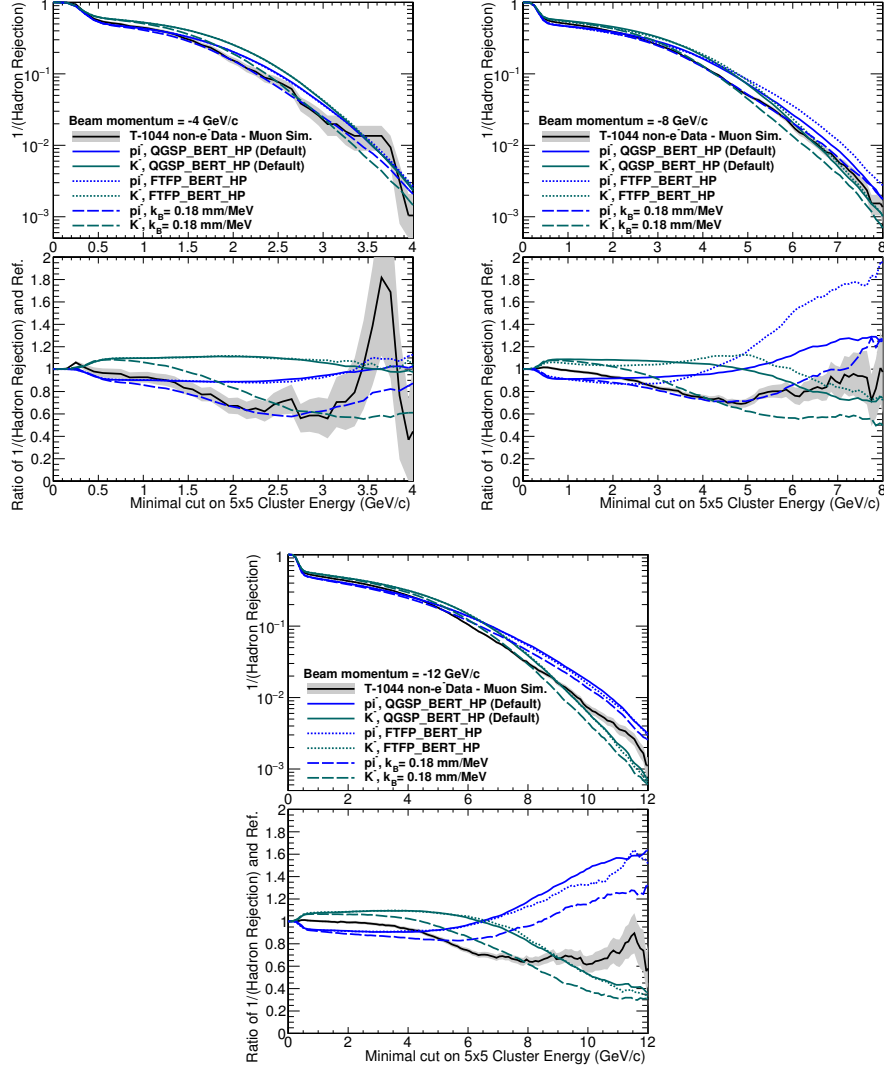


Figure 33: Hadron rejection plotted against minimal cuts on 5×5 tower cluster energy for beam momentum of 4, 8 and 12 GeV/c. The T-1044 hadron data (black curve with statistical uncertainties in gray), which are non-electron data with the expected muon contribution subtracted, are compared with π^- and K^- simulated curves with three simulation tunes, QGSP_BERT_HP physics list [19] with $k_B = 0.0794$ mm/MeV [22] (solid color lines), FTFP_BERT_HP physics list with $k_B = 0.0794$ mm/MeV (dotted lines) and QGSP_BERT_HP physics list with $k_B = 0.18$ mm/MeV [23] (dash lines). The beam momentum spread of around 2% is not unfolded and is present in both data and simulation.

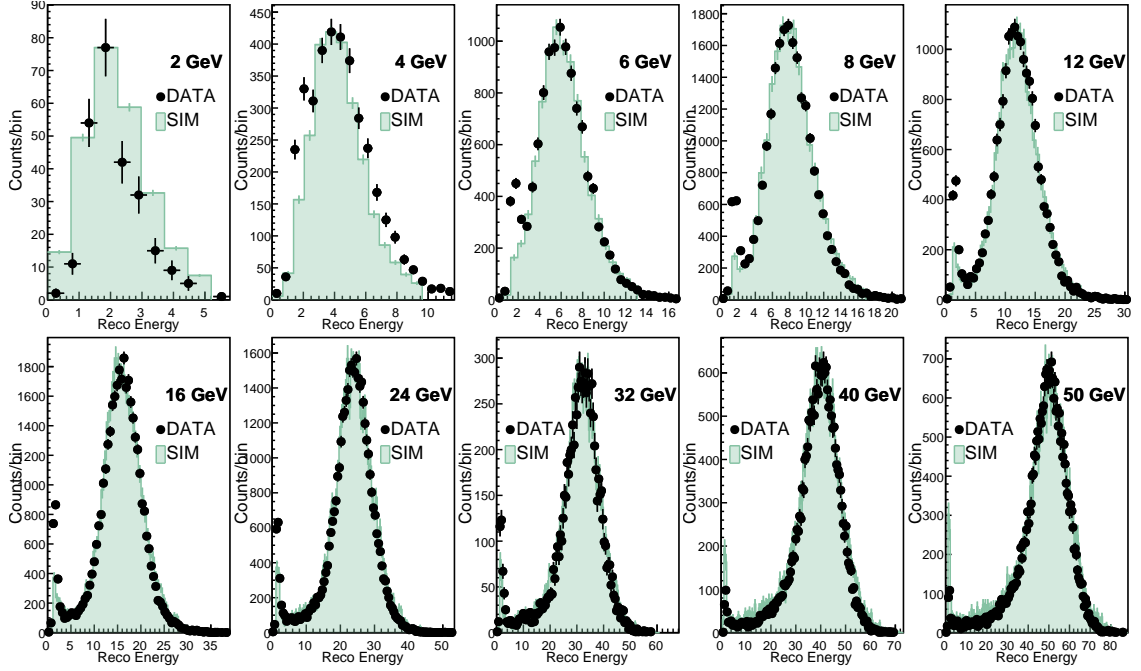


Figure 34: Hadron reconstruction in HCal standalone setup

7.2. HCal

The HCal standalone data are collected with only inner and outer sections of HCal in the beam line and no EMCAL in the front. The beam is adjusted to be in the middle of the prototypes in order to maximize the hadron shower containment in the 4×4 inner and outer HCal towers. Energy from all of the towers from both the inner and outer HCal are added together to determine the reconstructed energy. Electromagnetic showers generally start earlier in the calorimeter and deposit most of their energy in the inner HCal. The hadronic showers, however, are developed longitudinally deeper than electromagnetic showers and deposit most of their energy in the outer HCal.

Data were collected for beam energies between 2 GeV and 50 GeV which contain both electrons and pions. Electron and pion events were pre-selected with offline cuts using the two beamline Cherenkov counters. We applied hodoscope and veto cuts depending on the beam location, similar to the EMCAL analysis, but found no large dependence of the energy resolution on the beam position. Both high and low gain signals were collected but only low gain channels are used for analysis. Tower to tower calibration is

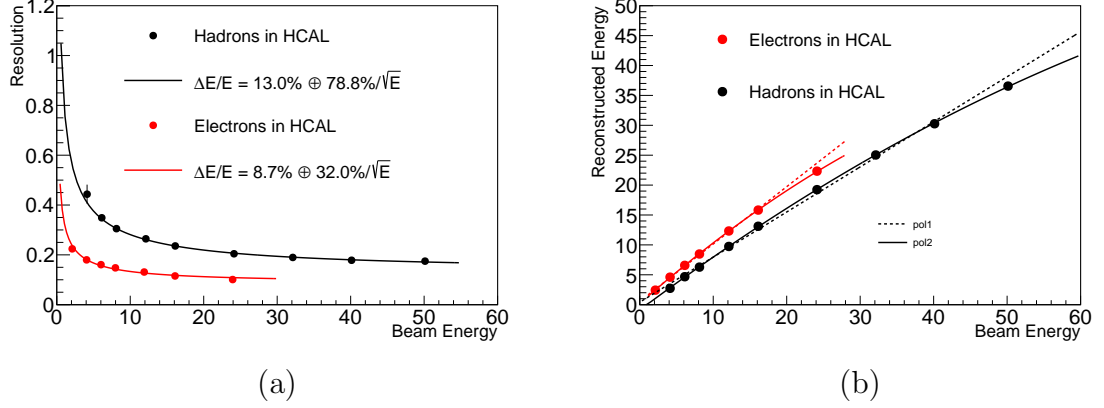


Figure 35: HCal Standalone (a) Resolution and (b) Linearity for electrons and hadrons.

done with cosmic muon events as discussed in Section 3. The inner and outer sections of the HCal are balanced such that the reconstructed energy should not depend on the energy asymmetry between the two sections. This procedure results in a weight factor of 2 that is applied to the inner HCal across all beam energies. This could be due to the fact that we have used cosmic muons for our calibration in addition to a constant sampling fraction obtained from GEANT4 for the energy scale.

Figure 34 shows a comparison of the reconstruction hadron energy between data and simulation. The simulation (filled histogram) and data (solid points) are in excellent agreement for 6-50 GeV beam energies. At lower energies the beam momentum spread increases, which has not been unfolded. The peak at the lower energies in the data corresponds to the small fraction of muons events that MIP through the HCal. The high side tail at the lower energies corresponds to the radial leakage, higher shower fluctuation and higher e/h ratio while the low side tail at the higher energies mainly corresponds to the longitudinal leakage. The corresponding hadron resolution and linearity are shown in Figure 35. The hadron energy resolution follows an empirical formula $13.0 \oplus 78.8\%/\sqrt{E}$, which matches the expected resolution from simulations very well. The large constant is due to the fact that the thickness of the steel plates increases longitudinally. Normal longitudinal fluctuations in the hadron shower development are enhanced by the fact that particles entering the calorimeter through gaps will traverse several extra cm in the steel absorber at the back than the front.

As seen in Figure 35(b), the energy response is not strictly linear. A second order polynomial shows good agreement with the data. The non-linearity is mainly due to optical saturation of the SiPM. For completeness, the electron resolution and linearity are also shown in Figure 35. The electron resolution is found to be $8.7 \oplus 32.0\%/\sqrt{E}$. This demonstrates the HCal's ability to assist the EMCal by measuring the electron energy leaking from the EMCal into HCal. The electron linearity follows a similar trend as that of the hadrons. The ratio between hadron and electron linearity corresponds to the e/π response of the calorimeter.

7.3. Hadron Measurement with sPHENIX configuration

The full hadron measurement is done with the sPHENIX configuration, which includes all three segments of calorimeters including the EMCal in front of the HCal. In this configuration the total energy will be reconstructed by summing up the digitized data from both the EMCal and HCal. The development of hadronic showers is a complicated process with significant fluctuations of the reconstructed energy compared to electromagnetic showers. The deconvolution of the shower starting position helps to exclude some of those longitudinal shower development fluctuations.

The events are sorted into three categories depending on their longitudinal shower profile:

- HCALOUT: Events where hadron showers MIP through the EMCal and inner HCal. These showers are developed primarily in the outer HCal alone or MIP through the full calorimeter system. These events are shown as the blue curve in Figure 36.
- HCAL: Events where hadron showers MIP through the EMCal. In these events, hadron showers start either in the inner HCal or outer HCal or MIP through all three calorimeters. These events are shown as red points in Figure 36.
- FULL: This represents all hadron showers irrespective of their starting point. They are shown as black points in Figure 36. These include hadron showers that start either in the EMCal, inner HCal, outer HCal or MIP through all three calorimeter systems.

These event categories help diagnose each section of the calorimeters independently as well as understanding of the leakage variations depending their starting position. As expected, the fraction of HCAL or HCALOUT

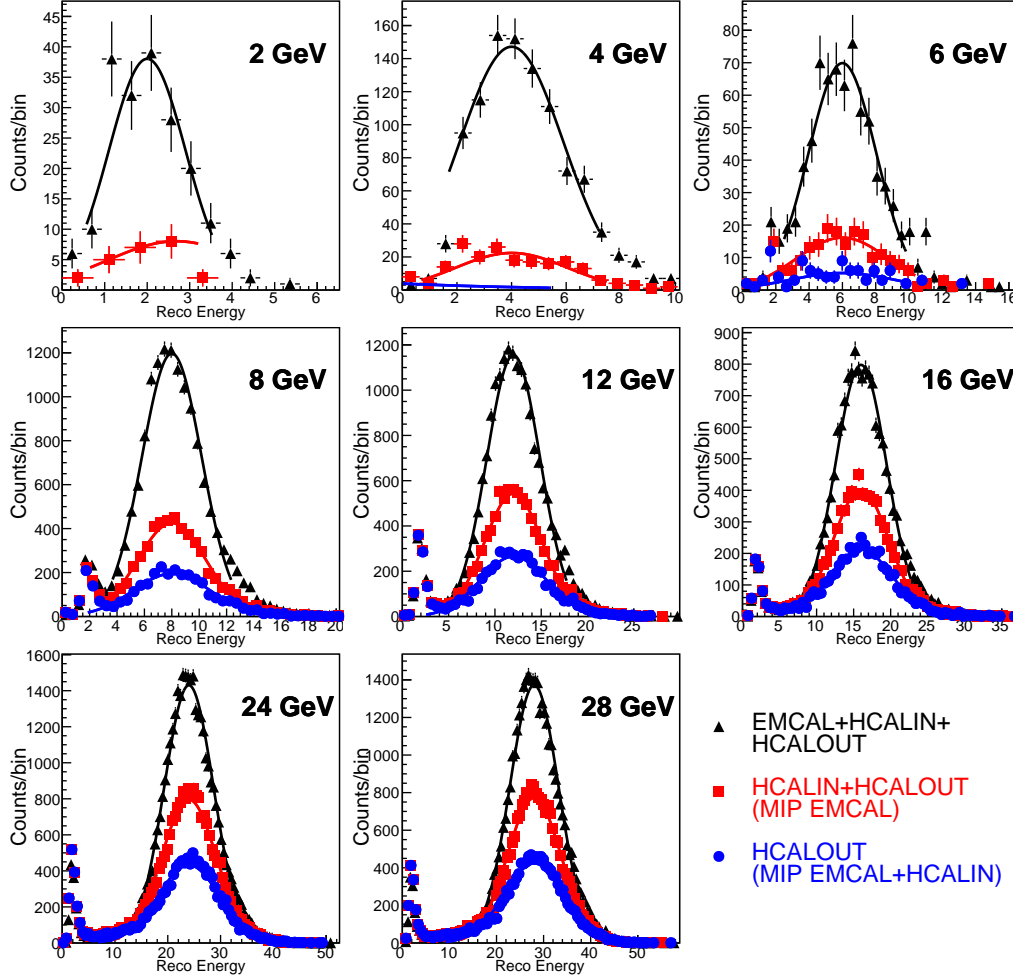


Figure 36: Hadron Energy distributions

events increases as a function of beam energy. The depth of the combined
 EMCAL+HCal system is $\approx 5.5\lambda$, which is not enough to fully contain all
 hadronic showers, so its response is systematically shifted from the input
 energy. Showers that start in the EMCAL have smaller leakage than show-
 765 ers that start in the outer HCal. Figure 37 shows a very good agreement
 between data and simulation. The data points represent all the hadron
 events and the simulation corresponds to the GEANT4 energy spectra of
 770 pions as reconstructed in data using the same code. The peaks at the lower
 energy corresponds to the small muon contamination events in the data
 but not simulated in the GEANT4. The corresponding hadron resolution is

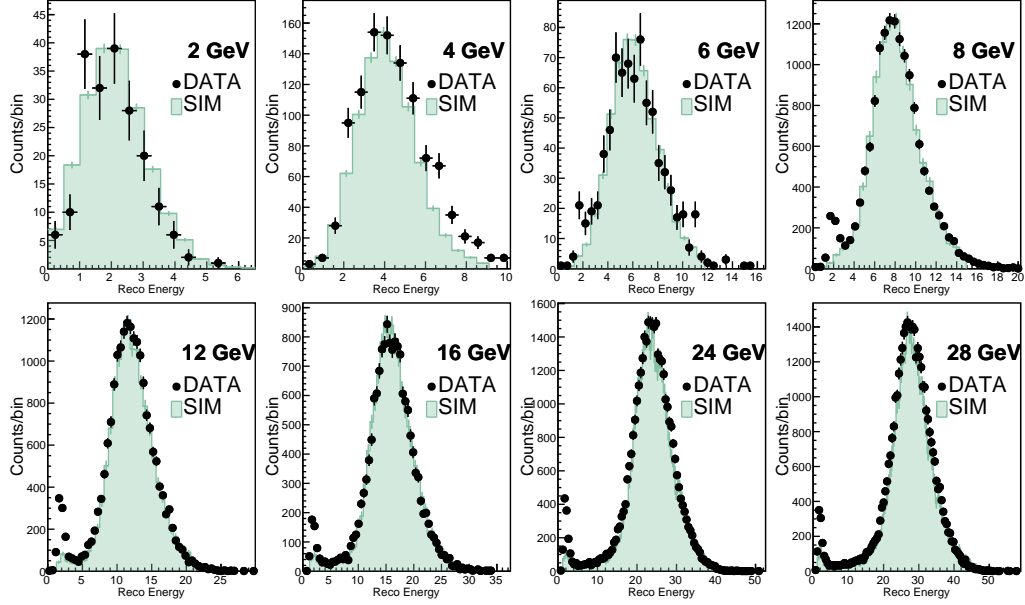


Figure 37: Data and Monte-Carlo matching of the hadron signal distributions

shown in Figure 38. An empirical parametrisation of the energy resolution is extracted both from data and simulations. The resolution corresponds to three data categories and two GEANT4 physics lists are in very good agreement.

8. Conclusions

A prototype of the sPHENIX calorimeter system was successfully constructed and tested at the Fermilab Test Beam Facility with beam energies in the range of 2-64 GeV. The energy resolution and linearity of the EMCal and HCal were measured as a combined calorimeter system as well as independently. The energy resolution of the HCal is found to be $\Delta E/E = 13.0\% \oplus 78.8\%/\sqrt{E}$ for hadrons. The energy resolution of EMCal for electrons is $2.6\% \oplus 12.3\%/\sqrt{E}$ for EM showers that hit at the center of the tower and $3.6\% \oplus 15.3\%/\sqrt{E}$ without the position restriction. Part of the EMCal position dependence of the shower response stems from the non-uniformity of the light collection in the light guide, which will be a major focus of the next stage of R&D. The combined calorimeter system is complicated by hadrons that start to shower in the EMCal. The calibrations are described in section 3.4. The combined resolution of the full EMCal and

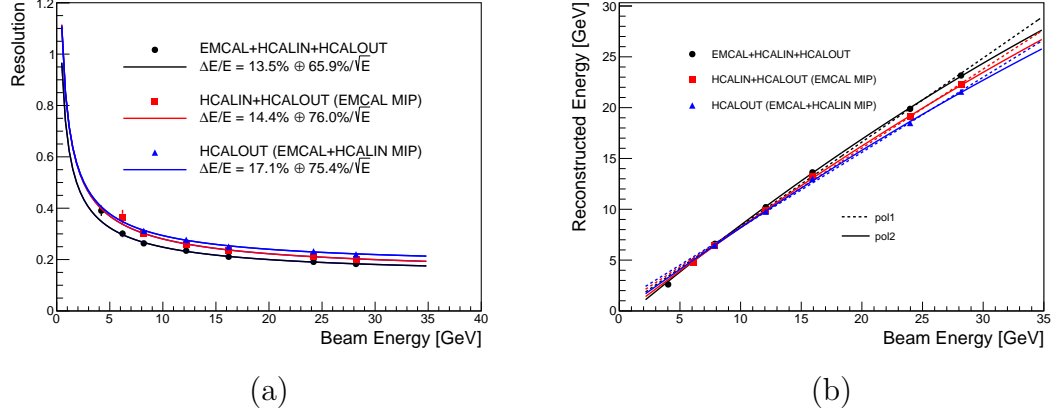


Figure 38: Hadron (a) Resolution and (b) Linearity for sPHENIX configuration

HCal system for hadrons is presented in section 7.3 and is consistent with the standalone HCal results. All of these results satisfy the requirements of the sPHENIX physics program. Excellent agreement between the test beam results and GEANT4 simulations is observed giving confidence to additional simulation studies in the final research and development of these detectors.

Acknowledgments

We wish to thank the staff of the Fermilab Test Beam Facility for their assistance with T-1044 operations. We also want to thank the technical staffs of the University of Illinois, Champaign-Urbana and Brookhaven National Laboratory for assistance in constructing the prototype detectors. This work was funded by the Department of Energy.

- [1] K. Adcox et al. Formation of dense partonic matter in relativistic nucleus nucleus collisions at rhic: Experimental evaluation by the phenix collaboration. *Nucl. Phys.*, A757:184–283, 2005.
- [2] J. Adams et al. Experimental and theoretical challenges in the search for the quark gluon plasma: The star collaboration’s critical assessment of the evidence from rhic collisions. *Nucl. Phys.*, A757:102–183, 2005.
- [3] B. B. Back et al. The phobos perspective on discoveries at rhic. *Nucl. Phys.*, A757:28–101, 2005.
- [4] I. Arsene et al. Quark gluon plasma and color glass condensate at rhic? the perspective from the brahms experiment. *Nucl. Phys.*, A757:1–27, 2005.

- [5] O.D. Tsai, L.E. Dunkelberger, C.A. Gagliardi, S. Heppelmann, H.Z. Huang, et al. Results of & on a new construction technique for W/ScFi Calorimeters. *J. Phys. Conf. Ser.*, 404:012023, 2012.
- 815 [6] O. D. Tsai et al. Development of a forward calorimeter system for the STAR experiment. *J. Phys. Conf. Ser.*, 587(1):012053, 2015.
- [7] B. D. Leverington et al. Performance of the prototype module of the GlueX electromagnetic barrel calorimeter. *Nucl. Instrum. Meth.*, A596:327–337, 2008.
- [8] S. A. Sedykh et al. Electromagnetic calorimeters for the BNL muon (g-2) experiment. *Nucl. Instrum. Meth.*, A455:346–360, 2000.
- 820 [9] T. Armstrong et al. The E864 lead-scintillating fiber hadronic calorimeter. *Nucl. Instrum. Meth.*, A406:227–258, 1998.
- [10] R. D. Appuhn et al. The H1 lead / scintillating fiber calorimeter. *Nucl. Instrum. Meth.*, A386:397–408, 1997.
- 825 [11] D. W. Hertzog, P. T. Debevec, R. A. Eisenstein, M. A. Graham, S. A. Hughes, P. E. Reimer, and R. L. Tayloe. A HIGH RESOLUTION LEAD SCINTILLATING FIBER ELECTROMAGNETIC CALORIMETER. *Nucl. Instrum. Meth.*, A294:446–458, 1990.
- [12] A. Izmaylov et al. Scintillator counters with WLS fiber/MPPC readout for the side muon range detector (SMRD) of the T2K experiment. *Nucl. Instrum. Meth.*, A623:382–384, 2010.
- 830 [13] W. Anderson et al. Design, Construction, Operation and Performance of a Hadr on Blind Detector for the PHENIX Experiment. *Nucl. Instrum. Meth.*, A646:35, 2011.
- [14] Martin L. Purschke. RCDAQ, a lightweight yet powerful data acquisition system. http://www.phenix.bnl.gov/~purschke/rcdaq_doc.pdf, 2012.
- 835 [15] The fermilab test beam facility. [online] <http://ftbf.fnal.gov/beam-delivery-path/>.
- [16] Nils Feege. Low-energetic hadron interactions in a highly granular calorimeter. *PH.D Thesis, Universit t Hamburg*, January 2011.
- [17] M. Blatnik et al. Performance of a Quintuple-GEM Based RICH Detector Prototype. *IEEE Trans. Nucl. Sci.*, 62(6):3256–3264, 2015.
- 840 [18] Aphetche et al. The PHENIX calorimeter, 2003.
- [19] S. Agostinelli et al. GEANT4: A Simulation toolkit. *Nucl. Instrum. Meth.*, A506:250–303, 2003.
- [20] sPHENIX collaboration. sphenix software repository. <https://github.com/sPHENIX-Collaboration>, 2015.
- 845 [21] J. B. Birks. Scintillations from Organic Crystals: Specific Fluorescence and Relative Response to Different Radiations. *Proc. Phys. Soc.*, A64:874–877, 1951.
- [22] M. Hirschberg, R. Beckmann, U. Brandenburg, H. Brueckmann, and K. Wick. Precise measurement of Birks kB parameter in plastic scintillators. *IEEE Trans. Nucl. Sci.*, 39:511–514, 1992.
- 850 [23] Alexander Tadday. Birks Coefficient of the AHCAL Scintillator. *CALICE Collaboration Meeting*.